

Accepted Manuscript

Comparison of 2-D and 3-D shape analysis of concrete aggregate fines from VSI crushing

Rolands Cepuritis, Edward J. Garboczi, Stefan Jacobsen, Kenneth A. Snyder

PII: S0032-5910(16)30905-6
DOI: doi: [10.1016/j.powtec.2016.12.037](https://doi.org/10.1016/j.powtec.2016.12.037)
Reference: PTEC 12185

To appear in: *Powder Technology*

Received date: 5 July 2016
Revised date: 29 October 2016
Accepted date: 10 December 2016



Please cite this article as: Rolands Cepuritis, Edward J. Garboczi, Stefan Jacobsen, Kenneth A. Snyder, Comparison of 2-D and 3-D shape analysis of concrete aggregate fines from VSI crushing, *Powder Technology* (2016), doi: [10.1016/j.powtec.2016.12.037](https://doi.org/10.1016/j.powtec.2016.12.037)

This is a PDF file of an unedited manuscript that has been accepted for publication. As a service to our customers we are providing this early version of the manuscript. The manuscript will undergo copyediting, typesetting, and review of the resulting proof before it is published in its final form. Please note that during the production process errors may be discovered which could affect the content, and all legal disclaimers that apply to the journal pertain.

Comparison of 2-D and 3-D shape analysis of concrete aggregate fines from VSI crushing

Rolands Cepuritis ^{a,b,*}, tel.: +47 95133075, rolands.cepuritis@norcem.no

Edward J. Garboczi ^c, edward.garboczi@nist.gov

Stefan Jacobsen ^a, stefan.jacobsen@ntnu.no

Kenneth A. Snyder ^d, kenneth.snyder@nist.gov

^a Department of Structural Engineering, Norwegian University of Science and Technology, NO-7491 Trondheim, Norway

^b Norcem AS (HeidelbergCement), R&D Department, Setreuveien 2, Postboks 38, NO-3950 Brevik, Norway

^c National Institute of Standards and Technology, Boulder, CO 80305, United States

^d National Institute of Standards and Technology, Gaithersburg, MD 20899, United States

Abstract: The shape of concrete aggregate fine particles (fines), with particle sizes between 3 μm and 250 μm , produced by high-speed vertical shaft impact (VSI) crushing of 10 different rock types from quarries in Norway, has been studied by both dynamic image analysis (DIA), which is a two-dimensional (2-D) method, and X-ray computed microtomography (μCT) coupled with spherical harmonic (SH) analysis, which is a three-dimensional (3-D) method. The 3-D μCT results serve as a check on the 2-D DIA results. The intent was to evaluate the applicability of the 2-D DIA method to extract shape parameters that could represent the actual 3-D shape of the VSI crushed concrete aggregate particles. The results show that the 2-D DIA method has problems correctly measuring the shape of particles smaller than about 40 μm due to too large of a pixel size and possibly some particle flocculation. The findings of this paper show, however, that if a large enough number of particles are analysed by the 2-D DIA method, a good but limited indication of the actual 3-D shape of the irregular crushed aggregate fines larger than 40 μm can be acquired and used for simple quality control in hard rock quarries.

Partial contribution of NIST – not subject to US copyright

Keywords: Crushed aggregate fines; vertical shaft impact crusher; shape; dynamic image analysis; X-ray computed tomography

1. INTRODUCTION

The interest in and need for increasing the use of crushed sand for concrete production are steadily growing due to shortages of suitable natural sand, as explained in Refs. [1], [2], [3], [4], [5]. However, natural sand, which may be weathered, differs from most fine crushed aggregates (crushed sand) in its grading, particle shape and surface texture [1]. Compared to natural sand, crushed fine aggregates incorporate significantly more fine¹ particles (also interchangeably referred to as filler or powder or fines in this paper), have different particle size distributions (PSDs), and tend to have particles that are more angular and often have rougher surfaces [1]. This affects the performance of the crushed sand in concrete, especially in terms of fresh concrete rheology (see [6], [7], [8], [9], [10], [11], [12], [2], [13]). Concrete performance is significantly affected by the volume fraction and characteristics of the fines in the crushed sand, including PSD, mineralogical composition, and shape [14].

Vertical shaft impact (VSI) rock-on-rock crushing is a popular technique used for improving (*i.e.* making more equi-axed) the shape of crushed sand particles, as part of the last comminution stage [16], [6], [17], [18]. VSI crushing seems to affect the particle size distribution down to about 36 μm [21], [22], [23]. The disadvantage is that it produces larger amounts of fines than does the more common cone crusher technology [22], because the dominant size reduction mechanism is attrition and impact [22]. Several VSI processing variables affect the shape of the product particles, such as VSI rotor speed, cascade flow, and influence of a closed circuit, as well as rock characteristics such as mineralogy, resistance to fragmentation, and feed size [27]. The aggregate and concrete production industries therefore need a fast, inexpensive, and reliable test method for product development and quality control of the fine (also defined as $\leq 250 \mu\text{m}$) crushed aggregate particles.

Well-established test methods for aggregate shape are available for particles larger than about 1 mm [7], [28], [29], [30], but there is a lack of industrial test methods suitable for smaller particles. The shape of the crushed concrete aggregate fines is usually described, for research purposes, by the so-called F-shape parameter (see [2], [21], [22], [23], [31], [32]). The F-shape parameter is defined to be the ratio between the maximum and minimum Feret diameters $x_{F\text{max}}$ and $x_{F\text{min}}$ (Figure 1), which are the maximum and minimum distances,

¹ The particle size definition of concrete aggregate fines is diverse. According to EN 12620 [61], fines are all material less than 63 μm . ASTM standard C33 / C33M – 13 [62] has a similar limit of 75 μm . For practical concrete purposes, however, it is most common to denote fines as all material less than 125 μm [63] or 250 μm [64].

respectively, between pairs of parallel tangents in a 2-D particle image [33] (thus the shape description is based on 2-D projections of actual 3-D particles). The parameters are determined from analysis of 2-D microscope images of polished sections of particles cast in epoxy. Typically, only about 100 to 200 particles are analysed in this test [21]. The smallest reported particle size analysed by this test method was 36 μm [23]. Particles smaller than 36 μm were not analysed because it is a difficult task to mechanically divide them into narrow size fractions. However, analysing wide size fractions requires analysing many more than only 100 to 200 particles to get a statistical representation of the particle shape. Obtaining such many-particle images would be laborious. This problem could be solved by the aid of Automated Scanning Electron Microscopy (ASEM), which can be used to rapidly investigate thousands of very fine particles. However, the results obtained would still be only 2-D images [34], [35], [36] giving limited information on the actual 3-D shape of the irregular crushed aggregate fines particles. It is also possible that these results could be biased by particle orientation in the sample preparation process. Preparing samples for the ASEM is also still laborious and time consuming and the method requires relatively sophisticated and expensive analysis equipment (SEM or ASEM). This is why the ASEM method is at present not suitable for everyday application within the aggregate and concrete production industries.

A new development within the last fifteen years is the use of X-ray computed microtomography (μCT), coupled with spherical harmonic (SH) analysis, to mathematically describe the full 3-D shape of particles and compute almost any geometrical property of the particles in 3-D [37], [38], [39], [40], [41], [42], [43], [44], [45], [46], [47], [48], down to particles with volume equivalent spherical diameters (VESDs) as low as 3 μm [48]. The VESD is defined as the diameter of a sphere with the same volume as the particle considered. Cepuritis et al. [48] have reported analysing samples containing up to 250 000 particles for the powder size fraction of 20 μm to 125 μm and up to 5500 particles in the size range ≤ 20 μm . This latter number, 5500, can be easily increased by scanning more sections of a given sample using more μCT scanning time and more computer hours for determination of the SH coefficients. The drawbacks of the μCT and SH method are time consumption, which including sample preparation time ranging from 2 h to about 24 h, and the relatively high cost of the μCT scanning equipment.

An alternative method that only takes about 5 min to analyse a comparable number of crushed aggregate powder particles, using less costly equipment and virtually no special

sample preparation, is the Dynamic Image Analysis (DIA) method [48]. However, this method can only provide a limited amount of information about particle shape using 2-D measures. It still could be applicable for everyday quality control at crushed concrete sand production quarries and concrete production units, if the method were able to yield crushed aggregate powder 2-D shape parameters that can reliably describe their performance in fresh concrete. The first preliminary comparison of the particle shape analysis by 3-D μ CT SH and 2-D DIA of two concrete aggregate powder samples (particle size between 3 μ m to 125 μ m) indicated that the methods ranked the shapes of the particles in the same order [48].

This paper presents studies of the shape of VSI crushed concrete aggregate fines from 10 different Norwegian rock types, each in three size fractions, using the 3-D μ CT SH method and 2-D DIA method. Previous studies on the same materials [49], [50] have focused on in depth analysis of how the VSI crushing affects the 3-D particle shape of the fines, comparing this effect to coarser particles from the same rock types, devising alternate shape description parameters and studying particle size distribution and specific surface of the fine materials. The purpose of this present study is then to evaluate the applicability of the 2-D DIA method to extract shape parameters that describe the real particle shape by comparing to the actual 3-D particle shape as determined by a combination of X-ray μ CT and SH analysis.

2. MATERIALS AND METHODS

2.1. Materials

Fine aggregate powder materials used for the study were produced from 10 different blasted and crushed rocks with a nominal size range of about 4 mm to 22 mm. The rock types were chosen from 10 different quarries in Norway to represent a wide range of local geological variety with respect to mineralogy and with respect to mechanical properties. This included (Table 1) igneous (intrusive and extrusive), metamorphic, and sedimentary rocks that were both mono- and multi-mineralic. Further processing included high rotor tip speed (70 m/s) VSI crushing to generate fines and static air-classification of the crushed products into three distinct size fractions with approximately the following d_{10} to d_{90} ranges: 4 μ m to 25 μ m (fine), 20 μ m to 60 μ m (medium) and 40 μ m to 250 μ m (coarse) (Table 1). The parameter d_N is the diameter where N % of particles, by mass, have a smaller diameter than d_N .

The finest of the produced powder fractions (4 μm to 25 μm) included all the particles smaller than 4 μm generated during the crushing and

Table 1: Crushed rock fines used for the study.

afterwards extracted by air-classification. The particle size ranges produced were partly overlapping because of the air-classification process, where the initial feed material is divided into two products: coarse and fine. Separation in air-classification is characterized by a cut-size, which is a border between these fractions. Due to various stochastic factors (air turbulence, particle collisions), some fines get into the coarse product and vice versa, so that an exact, non-overlapping border between particle sizes is not achieved. More details can be found in [27]. In total, 30 different powder samples were produced (Table 2): three particle size ranges for each of the 10 rock types. Mineralogical composition of the powders was determined by quantitative X-ray diffraction (XRD) analysis on the 4 μm to 25 μm size fractions (Table 2) [49].

The VSI crushing and air-classification experiments are described in Ref. [27]. Detailed studies of the particle size distribution (PSD) and specific surface area of all the crushed fines are presented in Ref. [49].

Table 2: Mineralogical composition of the various rock types used, determined with quantitative XRD.

2.2. Methods

2.2.1. DIA (2-D method)

The 2-D DIA technique approach used the “Fine Particle Analyser^{*}” commercial equipment (FPA) [51]. A powder sample was placed into a feeding funnel after which it was dispersed by compressed air at 200 kPa. The powder fell under gravity and 2-D images of the free falling particles were taken by a high-speed camera with an optical magnification such that the pixel size in the digital images was 4.29 μm (Figure 2). The 2-D projections were then analysed by software provided by the equipment producer to compute a wide range of

* Commercial equipment, instruments, and materials mentioned in this paper are identified in order to foster understanding. Such identification does not imply recommendation or endorsement by the National Institute of Standards and Technology (NIST), nor does it imply that the materials or equipment identified are necessarily the best available for the purpose.

statistical and geometrical parameters. At least 260 000 particles were analysed for each of the samples. Particle size was described by the area equivalent circle diameter ($DA =$ diameter of a circle with an area equal to the area of the 2-D projection of the particle) and the maximum and minimum Feret diameters x_{Fmax} and x_{Fmin} . The parameter to describe the irregular shape of the particles was then the ratio x_{Fmax}/x_{Fmin} , defined as the 2-D L/W (length/width) ratio. The 2-D L/W value can then be used to compare to the corresponding 3-D L/W value defined in the μ CT SH method, as discussed in Section 2.2.2 [48].

Figure 1: 2-D size parameters – maximum (x_{Fmax}) and minimum (x_{Fmin}) Feret diameters [33].

Figure 2: Screen-shot from the DIA image analysis software: displaying the captured 2-D shapes for some of the T10-3 crushed filler particles in the DA range of 200 μ m to 250 μ m and L/W > 1.5.

The precision of the instrument for the average of various measured shape properties, for the same sample analysed in replicate sequential runs, was determined to be well within ± 1 % standard deviation for each size subclass. A higher degree of variation (up to a standard deviation of 1.9 %) was observed when several subsamples were obtained from the same sample. The mean L/W ratios determined for different subsamples of the same powder type varied by ± 0.02 .

2.2.2. X-ray μ CT combined with spherical harmonic analysis (3-D method)

Combining X-ray μ CT with SH analysis for particle size and shape measurements has been discussed in [37], [38], [39], [40], [41], [42], [43], [44], [45], [46], [47], [48] and has been applied to similar crushed aggregate materials in [48] and [52]. Samples of the crushed powders were cast in epoxy at about 5 % volume concentration, (Figure 3) and the epoxy was hardened without settling by curing under rotation. Dispersion of the particles in the epoxy resin was obtained by vigorous manual agitation. Plastic tube moulds were used that had an outer diameter of 3 mm for the fine powder fractions (4 μ m to 25 μ m) and an outer diameter of 6 mm for the medium (20 μ m to 60 μ m) and coarse (40 μ m to 250 μ m) powder fractions. The mixture of epoxy and crushed powder was sucked into the tubes with a small vacuum pump. It was found to be advisable to use translucent plastic tube moulds, which enabled visual monitoring and thereby control of the sample-filling process.

After hardening, the samples were scanned using μ CT equipment, which gave 3-D images of all particles within the limitation of the voxel size used. Particles down to the volume of $8 \times 8 \times 8 = 512$ voxels were used for the shape analysis. This lower limit was employed since particles with volumes smaller than 512 voxels, or about 8 voxels in each direction, do not contain enough detail of the true particle shape to be worth computing SH coefficients. A few percent of those particles analysed were automatically eliminated by error-correcting software, usually because of touching particles that were interpreted as multi-particles. The μ CT equipment used was a Bruker Skyscan 1172 benchtop scanner, used for the 20 μm to 60 μm and 40 μm to 250 μm size fractions, and a Zeiss XRM500 Versa instrument, used for the 4 μm to 25 μm size fractions. The image size, pixel size, smallest analysed particle sizes, and number of analysed particles that generated valid SH coefficients are listed in Table 3.

Figure 3: Sample preparation for μ CT scanning; (a) 5 % volume of crushed powder on top of epoxy resin prior to dispersion; (b) homogeneous mixture of crushed powder dispersed in epoxy; (c) plastic tube mould and a hardened sample prior to μ CT scanning.

The resulting 3-D image, made by stacking many 2-D images, is a gray-scale image that needs to be segmented to produce the final 3-D image. In the segmented 3-D digital image, details below the voxel size have been lost, and it is possible that the volume of the particles in the image could be a little smaller or a little larger than reality, due to the choice of threshold used in the segmentation process. However, for larger particles whose volumes could be easily experimentally measured, this technique did give an accurate value (1 % to 2 % uncertainty) of particle volume [39]. There can be errors in the SH coefficients due to “ringing” effects in the actual SH coefficients, akin to the Gibbs’ phenomenon in 2-D Fourier series [53], [54], but these errors for random particles mainly affect derivatives on the particle surfaces, used in surface area and curvature computations. Since the shape parameters used in this paper, including volume, do not make use of surface derivatives, the ringing affects were neglected. SH functions [55] were generated using the X-ray μ CT data for each of the analysed particles. By using these functions, one can compute any geometric quantity of the particle, which can be defined by integrals over the volume or over the surface or any other algorithm using points on the particle surface or within the particle volume, since the SH approach gives an analytical, differentiable mathematical form for the surface [55], [53], [54].

The VESD was used to describe the average particle “size” and was computed from the SH analysis as defined in Ref. [55]. To give a measure of particle shape, the length (L), width (W), and thickness (T) can be defined (ASTM 4791 [56]). These are also quite similar to the set of three orthogonal distances used in sedimentary geology [53], [57]. L is defined as the longest surface-surface distance on the particle, W is defined similarly, but the line segment that defines W must be perpendicular to the line segment that defines L, and T is the longest surface-surface distance whose line segment is also perpendicular to both L and W. All these dimensions are computed from the SH analytical form for each particle [39]. Of course, after determining L and W, the direction, but not the length, of the T line segment is fixed. The two independent aspect ratios, L/T and L/W, can be used to calculate a characteristic aspect ratio of a particle, since L, W, and T define a rectangular box that just encloses the particle. The average over many particles of the value of the 3-D L/W can be compared to the corresponding many-particle average of the 2-D L/W value defined by the DIA method [48]. The mean L/W ratios for different subsamples of the same particle type varied by ± 0.02 for both 2-D and 3-D measurements [48]. Note that the same X-ray μ CT data could also have been analysed with a principal components analysis (PCA) method [58], [59] which would produce similar measures of particle dimensions. However, the results of the analysis of Refs. [58], [59] would not be identical to the L, W, T computations herein, since different algorithms are used to define these lengths. The principal axes of each particle, as determined by PCA, are not necessarily aligned with the axes defining L, W, and T. For this paper, since only ratios of L, W, and T are used as shape parameters, the PCA analysis may have been sufficient. If other shape parameters were needed, for example, those involving the curvature, the extra data that can be calculated from the SH analysis would be essential.

Table 3: μ CT and SH analysis – pixel size, smallest analysed particle size, image size and number of analysed particles.

3. RESULTS AND DISCUSSION

3.1. Shape characteristics as determined by 3-D μ CT scanning and spherical harmonic analysis method

Figure 4 illustrates the mean 3-D L/W ratios for all the different rock types and powder fractions, as determined by X-ray μ CT and SH analysis, plotted against the mean VESD of

the bins for which they have been determined. Particles larger than 12 μm and 150 μm have not been included in Figure 4a and Figure 4c, respectively, because for some of the ten rock types less than 100 particles fell in the bins above these sizes, which did not allow for a statistically valid result. An important observation from the plots in Figure 4 is that the mean shape characteristics, for each rock type, varied by less than 5 % over all the separate size bins. Another observation from results on Figure 4 is that the relative ranking of the mean values of L/W for different rock types seems to be preserved across the bins of the 8 μm to 120 μm size range when the size fractions (fine, medium and coarse) are considered separately. This is, however, less obvious in the case of the bin range of about 4 μm to 8 μm in Figure 4a and 120 μm to 150 μm in Figure 4b. For the case of the particles larger than 120 μm , the changes in the overall ranking of the shape might be attributed to the fact that only slightly over 100 particles were included in each bin, which might give a less statistically representative mean shape parameter of the bin. A bin was only analysed if there were at least 100 particles in it. In the case of particles smaller than 8 μm , the number of particles in one bin was at least an order of magnitude higher. However, as was discussed in [50], for these particles the influence of the crystallographic structure of the individual mineral on particle shape seems to be more influential than the VSI shaping process. These two observations were also found to be true in identical plots that used the L/T or the W/T ratios as shape description parameters (not included in the paper) [50]. This justifies the usefulness of mean shape parameters, which can be thought of as a single number representing the whole analysed powder sample over a fairly wide particle size range.

Figure 4: Mean L/W ratios of the analysed crushed powders, with the x-axis corresponding to the VESD of the median size of a bin: (a) 4 μm to 25 μm size fractions (shown to only 12 μm , see text); (b) 20 μm to 60 μm size fractions; (c) 40 μm to 250 μm size fractions (shown to only 150 μm , see text).

The relation between the mean 3-D shape parameter ratios (L/T, L/W and W/T) of the different rock types is presented in Figure 5. The data in Figure 5 show that the different shape parameters are related, which is shown by the relatively high values of the squared linear correlation coefficients, R^2 (all greater than 0.9 and most close to 1). Aschenbrenner's [60] shape factor F, determined from the mean values of the particle dimension, only varies from 0.87 to 1.02, with an average value of 0.95 and only one value exceeding 1.0 [50]. This suggests that most of the particles are quite equi-dimensional and not particularly prolate

(rod-shaped) or oblate (disc-shaped) [61]. It also means that it is reasonable to use only one of the determined ratios between the three orthogonal axes (L, W, T) in order to rank the different crushed powder samples in terms of their actual 3-D particle form. The 3-D L/W parameter was chosen in order to relate more closely to the 2-D L/W ratio as determined by the DIA method [48].

Figure 5: Relation between shape parameters L/T, L/W and W/T, as determined by 3-D μ CT scanning and SH analysis.

3.2. Shape characteristics as determined by 2-D DIA method

Figure 6 shows the mean 2-D L/W ratios, determined by the DIA method, plotted against the mean DA (area equivalent circle diameter) of each bin in the various size ranges. The range of equivalent particle sizes is wider for the DIA method in Figure 6 than for the corresponding results obtained by the μ CT SH method in Figure 4. One reason for this is because for the analysis by the 2-D DIA method no minimum limit of pixels was set in order to analyse the shape of a particle. This means that particles down to a single pixel size of 4.29 μm have been analysed for all the fractions. The second reason is that, in general, a much larger number of particles were characterised by the DIA measurements, especially for the 4 μm to 25 μm powders. Therefore, 2-D L/W statistically confident values were able to be obtained for the smaller size bins in the 4 μm to 25 μm size range and for the larger bins in the 40 μm to 250 μm size range. Results were not calculated for these two bins for the μ CT results, since the number of particles in these bins analysed by μ CT was below 100, which did not allow for a statistically valid result (see the discussion above).

Figure 6: Mean L/W ratio of filler fractions as determined by 2-D DIA method; x-axis corresponds to the equal area circle diameter (DA) of the median size of a bin; (a) 4 μm to 25 μm fractions; (b) 20 μm to 60 μm fractions; (c) 40 μm to 250 μm fractions. The small illustrations on the top right corners of the plots show enlargements of the small DA data.

3.3. Relation between the shape parameters determined by the 2-D and 3-D methods

The results from Figure 4 and Figure 6 show that in the particle size range above about 40 μm VESD or DA the mean L/W ratios vary in a relatively narrow range of approximately 1.3 to 1.7, with the 2-D values being slightly higher. For particles with VESD < 40 μm , the 3-D

method results stay within the same range, while the 2-D L/W values indicate two sharp peaks at the small size end of the graphs (see Figure 6) for most of the analysed powder samples. These peaks occur at a DA value of about 17.5 μm , which is between the 15 μm and 20 μm bins, and then again at the 5 μm and smaller DA bin. The first peak at 17.5 μm is more pronounced and has a higher absolute value for the two finest particle size fractions (4 μm to 25 μm and 20 μm to 60 μm), as can be seen from Figure 6a and Figure 6b, *i.e.* in the case when more of the very fine particles were actually present in the analysed samples. The height of the second peak is at mean L/W = 3.4 for all three particle size ranges.

The two observed peaks in the DIA measurements also affect the mean value of the L/W ratios calculated for a whole particle sample, weighted by mass fraction. This is illustrated in Figure 7 where mean L/W ratios for all the samples are compared for the 2-D and 3-D methods. The mean 3-D L/W ratios (Figure 7a) are similar in magnitude for the three different particle size ranges. However, the mean 2-D L/W ratios in Figure 7b are only similar for the two smaller particle size ranges and are much lower for the coarsest particle size range. One must also note that a direct comparison of the relative results in Figure 6 and Figure 7 might be difficult, in particular for the results of the 4 μm to 25 μm size range. This is because only bins where there were more than 100 particles were included in the plots in Figure 7. For example, bins with particles larger than about 80 μm were not included in Figure 6a, but these particles were included in the calculation of the mean L/W ratios weighted by the mass fractions presented in Figure 7. Because of this weighting, these large particles would have a large effect on the mean L/W ratios.

Figure 7: Mean L/W ratio of the different crushed powder fractions; (a) 3-D μCT SH method results; (b) 2-D DIA method results.

Some random 2-D projections were extracted from the T5 rock type 4 μm to 25 μm size fraction (T5-1) in order to visually observe the DIA particle projections at the first peak, between 15 μm and 20 μm . The purpose was to evaluate whether any reason for the increased equi-dimensionality could be seen visually. Only particles with $15 \mu\text{m} < \text{DA} < 20 \mu\text{m}$ and $2.3 < \text{L/W} < 3.0$ were randomly chosen (see Figure 8). The T5-1 sample was selected as it has the highest peak of the L/W values for particles between 15 μm and 20 μm VESD (see Figure 6a). The same exercise was repeated for the 3-D μCT method results from the same T5-1 powder particles of the corresponding equivalent size. However, the range of the L/W ratios

of these particles went from 1.6 to 2.4, because no particles of a higher L/W ratio than 2.4 had been registered and very few with L/W exceeding 1.6. This is shown in Figure 9 where some examples of 3-D images (created with Virtual Reality Modelling Language, VRML) of the actual particles based on the SH method of approximating the shape [43], [55] are shown. A comparison of Figure 8 and Figure 9 shows that the level of detail for the actual appearance of the particle shape, achievable with the 2-D and 3-D methods for these very fine particles, is quite different. Artefacts affecting the determined shape parameters, such as touching multi-particles for example, can be made from the high resolution 3-D images in Figure 9. On the other hand, the level of detail in Figure 8 is too limited to determine the actual reason for the L/W peaks observed in Figure 6. By the naked eye, it appears that the 2-D images in Figure 8 are a bit more angular than the 3-D images in Figure 9. However, the low number of pixels per particle in Figure 8 does not provide enough shape detail in order to confidently describe the angularity with mathematical parameters.

Figure 8: Some 2-D images captured by the DIA equipment (T5-1 crushed fines sample; $15 \mu\text{m} < \text{DA} < 20 \mu\text{m}$; $2.3 < \text{L/W} < 3.0$).

Figure 9: 3-D VRML images of random particles based on the results from μCT scanning and spherical harmonic analysis (T5-1 crushed fines fraction; $10 \mu\text{m} < \text{VESD} < 20 \mu\text{m}$; $1.6 < \text{L/W} < 2.4$).

The reason for the two DIA peaks in the mean L/W plot for $\text{DA} < 40 \mu\text{m}$ (see Figure 6) is the formation of particle flocs due to inter-particle attractive forces of different types, such as adhesion and non-bonded van der Waals forces [62], [63], [64], [65], [66], [67]. These forces can be strong enough so that the flocs were not broken up by compressed air flow in the DIA equipment during the measurements. The preparation method for the μCT particle samples allows for proper de-flocculation (see Section 2.2). This means that during the DIA measurements, the very small particles could be adhering to the bigger ones and to each other. As the particle size gets smaller, the formation of the flocs has a larger effect on the measured particle shape. For example, two circular images, each of diameter D, with $\text{L/W} = 1$, when just barely attached to each other as in a floc, will now be a particle with $\text{L/W} = 2$. During the DIA measurements, the build-up of very small particles in the corners of the high-speed camera lens, when the $4 \mu\text{m}$ to $25 \mu\text{m}$ size fractions were analysed, was visually observed. This means that the particles were adhering to the glass and to each other and had to be wiped away after the measurement. One of the many digital images taken by the high-

speed camera during measurements on the T5-1 powder sample (Figure 10) illustrates this phenomenon.

A similar problem as shown in Figure 10 was noticed for all the other 4 μm to 25 μm samples analysed, with an exception of the T9-1 and T10-1 samples, which do not indicate these peaks in Figure 6a. Another study [49] on the PSD and specific surface area of the same materials showed that T9-1 and T10-1 were the two coarsest (having virtually none of the very small particles $\leq 5 \mu\text{m}$ equivalent size) samples in the nominal 4 μm to 25 μm particle size range. This implies a smaller flocculation potential as the dominance of the electrostatic forces decreases with increased particle size [62], [63], [64], [65], [66], [67]. It can also be noted that previous studies on the same [49] and similar materials [48] with respect to their PSD measurements revealed that the DIA method generally had limited ability for detecting particles smaller than about an equivalent size of 30 μm . This would imply that the number of particles counted below this size is reduced, as they form larger particles by either adhering to each other or to larger grains. Quantitative studies on the ability of certain crushed rock fines materials to form flocs is an interesting further research direction for better understanding the limitations of the DIA method.

Figure 10: A digital image taken by the high-speed camera during DIA measurements of the T5-1 crushed powder sample. The red outlines around the dark grey spots indicate detected projections of crushed powder particles that were used for the shape analysis. The light grey background represents the screen in front of which the particles are falling and the dark grey layer on the left side indicates build-up of very small particles in the corner of the high-speed camera lens.

In a previous study [48], we analysed SEM (Scanning Electron Microscope) micrographs of crushed aggregate powders originating from some of the same rock types as studied in this paper.

Figure 11 illustrates some micrographs obtained for the T1 and T2 rock type crushed powder particles of about 20 μm to 100 μm in size. From these micrographs, the existence of much smaller particles adhered to the surface of larger particles can be observed. Adhering small particles could affect both shape and size analysis depending on the method of analysis. When a layer of smaller particles is formed on a larger particle, the shadow dimensions of the large particle are increased and the L/W ratio could also be increased as was discussed previously.

Figure 11: SEM micrographs of crushed aggregate powders with possible smaller (1 μm to 10 μm) particles adhered to larger (20 μm to 100 μm) particles; (a), (b) T1 rock type; (c), (d) T2 rock type [48].

The two-peak structure in the DIA data occurs for values of DA below about 30 μm . At a pixel size of 4.29 μm , this size corresponds to about 7 pixels. In the 3-D X-ray CT data, the size of particles analysed was restricted to being greater than about 8 voxels. Therefore, the DIA peak structure is generated for particles that probably should not be analysed for shape, because of having too few pixels for valid results. The peak for DA below 5 μm , however, can probably be further explained by the 4.29 μm pixel size, since in this size range the value of W for most particles will almost always be one pixel, while the length L is determined by how many particles are adhered to each other. For the data sets that had very few particles registered for DA below 5 μm , T9-1 and T10-1, the peak at a DA value of 5 μm in Figure 6a was absent. Therefore, if we want to make 2-D vs. 3-D comparisons for the particles below about 20 μm in size, a different way of creating the 2-D projections needs to be carried out.

In order to understand whether the 2-D and 3-D methods are able to rank the different crushed powder samples in the same relative order with respect to their mean L/W ratios, and because of the issues discussed in the last paragraph, it was decided to use only the data obtained from analysing particles with VESD or DA > 40 μm . This decision excluded the peaks in Figure 6. A plot of the 2-D vs. 3-D mean L/W data for particles with VESD or DA > 40 μm in the size fractions 40 μm to 250 μm is presented in Figure 12. As can be seen from Figure 12, a reasonably good agreement between the two methods is achieved, within uncertainty. This is also illustrated by the relatively high squared linear correlation coefficient R^2 equal to about 0.8. However, the relation from Figure 12b also indicates that the 2-D mean L/W values are on the average about 10 % higher than the corresponding 3-D values. In Figure 12b, the correlation line was constrained to go through the origin, to better compare the 2-D and 3-D L/W ratios, since ideally both sets of measurements independently go through the origin. When evaluating the results in Figure 12, it might seem that the indicated error bars are large, and this would then reduce the practical meaning of this correlation between the 2-D and 3-D shape parameters. However, this is misleading, due to the scale of the axes of the plot in Figure 12, *i.e.* the results only include particles of very similar shapes where the mean L/W ratios vary in the range of +/- 0.07 units or about +/- 5 %. Thus, as this

correlation seems to work in the very narrow range of particle shapes, it is expected to be even more applicable to study particles where the shapes vary over a wider range.

Figure 12: Correlation between mean L/W ratios of the crushed fines particles of 40 μm to 250 μm size fractions as determined by 2-D DIA and 3-D μCT SH methods. The error bars represent the estimated repeatability of the test method, determined by analysing several sub-samples of the same powder type; (a) unrestrained linear regression; (b) linear regression constrained to pass through the origin.

When evaluating the results from Figure 12, one has to also take into account that the DIA shape results are based on image analysis of 2-D projections of 3-D particles. A 2-D vs. 3-D correspondence is almost never exact with the exception of perfectly spherical particles [68]. In addition, one has to bear in mind the different sample preparation and measurement principles of the two test methods and how the L/W shape parameters were determined. This is because L/W ratios determined by both 3-D and 2-D methods (Figure 4 and Figure 6) are based on different assumptions. L/W ratios determined by the 3-D method (Figure 4) are based on a real 3-D model of a particle, by defining a rectangular box with dimensions L, W, and T that just encloses the particle (see Section 2.2). This means that the three dimensions are mutually orthogonal and $L \geq W \geq T$. Therefore, $L/T \geq L/W$. L/W ratios determined by the 2-D method (Figure 6) are determined on a random 2-D projection of a particle described by the maximum and minimum Feret diameters x_{Fmax} and x_{Fmin} . As explained in Section 2.2, the Feret diameters are defined by the maximum and minimum distance between parallel tangents in a 2-D particle image (Figure 1), which are tangent only at points of positive curvature and which may not touch other parts of the particle image. These maximum and minimum distances are defined by line segments that are usually not orthogonal to each other.

The only way to be able to directly compare 3-D X-ray μCT results to 2-D optical scanning results, for individual particles and without algorithmic differences, is to use an algorithm that computes the 2-D projections from the 3-D results. This algorithm was developed to compute the projection of a particle, with origin at the centre of mass, onto the $z = 0$ plane. For a particle projected in the orientation as it was scanned in the X-ray μCT scanner, the z -direction is the direction perpendicular to the direction of scanning or parallel to the original plastic tube sample. However, different projections can be computed by first rotating the particle [53], [54] then computing the $z = 0$ projection. The algorithm is composed of several simple steps, illustrated by Figure 13. Because of the SH analysis, the particle surface is

represented analytically by the function $r(\theta, \phi)$, where θ and ϕ are the usual spherical polar coordinates. The angle θ is taken from the z axis, and the angle ϕ is taken from the positive x axis, and is positive in the counter-clockwise direction. Figure 13 shows a slice through a particle, taken along a direction ϕ . The axes are as shown. For the chosen value of ϕ , the distance from the z -axis to the 3-D particle surface, for a given value of θ , is $r(\theta, \phi) \sin(\theta)$, as is shown in Figure 13. The maximum of this quantity is found over the range $0 < \theta < \pi$ and is defined as $R(\phi)$, one point on the outer edge of the 2-D projection.. The collection of these lengths defines a function $R(\phi)$, which is the outline of the projection of the particle in the $z = 0$ plane. The function $R(\phi)$ is periodic and has no sharp edges or points, so can be used to compute a Fourier series in cosine and sine, in the same way as the 3-D X-ray μ CT data made possible a spherical harmonic series, resulting in an analytical and continuous curve for the projection [55].

Figure 13: Slice through a particle, taken along a direction ϕ .

Next, the maximum and minimum caliper distances (Feret diameters) are computed, illustrated in Figure 14, which is a 2-D projection of a particle like that shown in Figure 13. The circle in Figure 14a shows a region of the projection that has positive curvature, along with defining axes and the definition of $R(\phi)$. All the points of positive curvature of $R(\phi)$, within some resolution limit (a few hundred points) are computed and saved using a grid of points in ϕ . Caliper lines can only touch a planar object at points of positive curvature, where they are tangent lines. These positive curvature points are then checked to see if a line tangent to any of these points touches the projection in another place. Figure 14b shows a line segment that is tangent to a point of positive curvature that if extended does touch another part of the projection. This point is not saved. If the tangent line does not touch another point of the projection, which case is shown in Figure 14c, then this positive curvature point is saved. Pairs of all the tangent line slopes of this collection are compared and are treated as caliper pairs if their slopes are within 1 % of each other, making them parallel. The distance between each pair of lines is determined, using ordinary geometric formulas, and the minimum and maximum distances are found. These are then the minimum and maximum caliper distances (Feret diameters) for this projection, and their ratio can be directly compared to the DIA results.

Figure 14: A 2-D projection of a particle like in Figure 13.

The optical DIA scanner captures only a single projection of each particle and it is assumed by the manufacturer that there is no preferential orientation of particles during the particle dispersion process by the suspending compressed air used. By analysing a large enough number of randomly oriented particles the two measurement methods should yield similar mean L/W ratios.

A comparison of particle characteristics, as determined from the 3-D shape analysis and from the 2-D projections of the 3-D μ CT SH particle models, has been compiled for five T5-3 particles in Table 4. Shape characteristics of the five particles were first determined over the whole SH model surface in 3-D and then from 2-D projections in the $z = 0$ plane of the very same 3-D particle models. The data in Table 4 illustrate that for a limited number of particles, there indeed is no direct relationship between the actual 3-D L/W ratio and an L/W ratio of a random 2-D projection of the actual 3-D shape. Moreover, the L/W ratios as determined in 2-D from the Feret diameters (caliper distances; see column 7 in Table 4) can either be considerably increased (see particles No. 1 and No. 2 in Table 4) or decreased (see particles No. 4 and 5 in Table 4) compared to the actual 3-D values (see column 3 in Table 4), depending on the particle orientation during the imaging of the 2-D projections. It can then be anticipated that the relatively good correlation of the 3-D and 2-D data observed in Figure 12 will prevail, only if a large enough number of particles with no preferential orientation is analysed allowing for a good statistical representation of the particle shape characteristics. It can also be anticipated that fewer particles need to be analysed by the 3-D method to achieve this representation. This is because analysis by the 3-D method provides the true L/W ratio for each particle, while many different values can be obtained from the same particles in 2-D, depending on the actual orientation with respect to the plane of projection. To better understand this point, consider a collection of identical shape but different size tri-axial ellipsoids, all with their axis lengths in the ratios 1:1.5:3, so that $L = 3$, $W = 1.5$, and $T = 1$. A 3-D determination of L/W results in $3/1.5 = 2$, while looking at slices, L/W will range from 1.5 to 3, depending on how the ellipsoid is projected into a plane.

Table 4: Comparison of some particle characteristics of the T5-3 fines as determined from the 3-D shape analysis (columns 2-5) and from the 2-D projections of the 3-D μ CT SH particle models (columns 6-8). The 2-D projections in column 8 come from column 4 VRML images.

Figure 15 illustrates the mean L/W ratios obtained from the 2-D projections of the 3-D particle models for all the different rock types and powder fractions, plotted against the mean DA of the bins for which they have been determined. These projections were obtained from random rotation of the original 3-D particles as imaged in the X-ray μ CT. These L/W results can then be directly compared to the 2-D DIA results in Figure 6 and the 3-D results in Figure 4. It can be seen from Figure 15 that the two sharp peaks in the L/W ratios observed in Figure 6 at the particle size of about 17.5 μm (between bins of equivalent sizes 15 μm and 20 μm) and then again at the very small particle size bin described with the DA of slightly below 5 μm , are absent in the data extracted from the 3-D particle models. This would confirm that the reason for the appearance of the two peaks seems to be mainly connected to the pixel size of the high-speed camera in the DIA method, rather than flocs since any attached small particles seem to be small compared to the minimum DIA pixel size (see Figure 11). A comparison of Figure 4, Figure 6 and Figure 15 shows how the mean L/W ratios changed depending on the method of analysis. The mean L/W ratios of the 2-D projections of the 3-D particles, shown in Figure 15, had values (1.40 to 1.80) that were much closer to the DIA-determined 2-D L/W ratios (also 1.40 to 1.80, shown in Figure 6). The mean 3-D L/W ratios from the 3-D analysis, shown in Figure 4, ranged from 1.30 to 1.55. We wish to emphasize that these accurate results, especially for the smallest particles, were only made possible by directly computing the 2-D projections from the actual 3-D particles.

Figure 15: Mean L/W ratio of filler fractions as determined from the 2-D projections of 3-D μ CT SH results, x-axis corresponds to the equal area circle diameter (DA) of the median size of a bin; (a) 4 μm to 25 μm fractions; (b) 20 μm to 60 μm fractions; (c) 40 μm to 250 μm fractions.

The last question to be addressed is that of potential particle orientation in the various L/W measurements. The question of particle orientation does not apply to the 3-D measurements of L and W, since shape characteristics are determined over the actual surface of the 3-D particle. However, as was seen in Table 4, the orientation of a particle has a large effect on the shape of the 2-D projection, so any preferred spatial orientation in the actual 3-D particles could affect the mean 2-D L/W ratio values. This applies to both the DIA method and the 2-D projections from the X-ray μ CT SH method.

One way to assess any orientation effects in the DIA results is to take the actual L, W, and T values as measured by X-ray μ CT SH, and use these to generate, via numerical simulation,

sets of completely randomly oriented ellipsoids with their semi-axes matching the actual L, W, and T values. The 2-D projection of a randomly oriented ellipsoid with axes ($c \geq b \geq a$) is an ellipse with axes ($\lambda > \omega$). If we make ellipsoids with the same aspect ratios, as given by L, W, and T, as the real particles, then we can use the techniques of Ref. [69] to see what will happen with the average 2-D projections. By using ellipsoids, we can easily perform extensive averages over many projections. Therefore, the 3-D μ CT measurements of (L, W, T) for each particle measured were used to create an ellipsoid with axes ($c=L$, $b=W$, $a=T$). Each ellipsoid was rotated to a random orientation, and the 2-D ratio $\beta = \frac{\lambda}{\omega}$ was calculated from the length of the ellipsoid axes and the Euler angles defining the orientation [69]. The average value of β is an estimate for the average projected 2-D L/W value. The average ellipse L/W was calculated from the population of particles, and the entire calculation was repeated 20 times. The standard deviation in the calculated mean was always less than 0.01. Table 5, in the “DIA (L/W)” and “Ellipsoid (L/W)” columns, shows the results of this analysis. Excellent agreement is seen between these two datasets. Therefore, there are probably no preferred directions in the suspending airstream in the DIA method, since the generated ellipsoids were totally randomly oriented, implying that the particles in the DIA method were also totally randomly oriented.

We next consider the X-ray μ CT data. 2-D projections were prepared from each particle as it was oriented in the original sample. The mean values of the 2-D L/W ratio were computed and are presented in Table 5 in the “ μ CT (L/W), as scanned” column. In most cases, this data is significantly higher than either the ellipsoid or DIA data, implying that there could have been some degree of particle orientation as the particles, embedded in liquid epoxy, were sucked into the plastic tubes, due to viscous forces. The 3-D particle models were then randomly rotated, and the mean L/W ratios re-computed. This data is presented in Table 5, in the “ μ CT (L/W), random angle average” column, and is now found to agree much more closely with the ellipsoid and DIA data. We conclude that there were indeed particle orientation effects on the 2-D projections of the 3-D shape data. These effects can be removed by randomly orienting the 3-D particle models before computing 2-D projections.

Table 5: Comparison of measured and calculated shadow (L/W) ratios for particles of 40 μ m to 250 μ m fractions using dynamic image analysis (DIA), μ CT particles suspended in epoxy with and without orientation averaging, and ellipsoids having major axes equal to the major axes calculated from the μ CT particles. The last column indicates the number of μ CT particles used in the calculation.

Figure 16 presents the final comparison between the 2-D DIA results and the 2-D X-ray μ CT SH results, with random rotations of each particle. The regression line was forced to go through the origin. The trend line equation is $y = 0.9793 \cdot x$, where x is the mean L/W ratio obtained from the 2-D projections of the randomly-oriented 3-D μ CT SH particle models and y is the mean L/W ratio, as obtained by the 2-D DIA method. This slope of this trend line is very close to unity, as it ideally should be, if all particle orientation effects are removed and a sufficient number of pixels per particle size (about eight or more) is used.

Figure 16: Linear regression constrained to pass through the origin between mean L/W ratios of the crushed fines particles of 40 μ m to 250 μ m fractions as determined by 2-D DIA and from the 2-D projection of the randomly-oriented 3-D μ CT SH particle models. The error bars represent the estimated repeatability of the test method, determined by analysing several sub-samples of the same powder type, and the slope of the regression line is 0.98.

4. CONCLUSIONS

The following conclusions can be drawn from this study:

- There are problems correctly detecting separate particles and measuring their shapes for grains smaller than about 40 μ m of equivalent diameter in the DIA measurement method. This is due to the rather large pixel size used in the DIA method, 4.29 μ m. Using a smaller pixel size would allow the shape of smaller particles to be accurately measured. Thus the actual resolution of the 2-D DIA method is an order of magnitude lower than for the 3-D μ CT SH approach, which was demonstrated to be able to investigate particles down to a VESD value of about 3 μ m;
- The available level of particle shape detail is much higher for the 3-D μ CT SH approach than is obtainable with the 2-D DIA method used;
- The outcome of any method based on particle shape measurements taken from 2-D projections of irregular 3-D particles, is dependent on the particle orientation during the imaging process, while particle orientation during the 3-D μ CT SH does not affect the 3-D result. This means that significantly fewer particles need to be analysed by the 3-D μ CT SH method in order to obtain a representative average result, since no averaging over projection direction is needed. No particle orientation effects were seen in the DIA method, while there was some particle orientation in the plastic tube samples used in the X-ray μ CT method, due to viscous forces when the epoxy-particle

mixtures were sucked into the tubes. These particle orientation effects on the computed 2-D projections was overcome by randomly orienting the particles before 2-D projections were made;

- If enough particles larger than $DA = 40 \mu\text{m}$ are analysed by the 2-D DIA method, a good limited indication of the actual 3-D shape of the irregular crushed aggregate fines particles can be acquired. At this size, there are enough pixels across each particle, for a pixel size of $4.29 \mu\text{m}$, to achieve valid shape measurements. For this size particle and larger, the effects on the computed shape of much smaller particles sticking onto the particle, as was seen in Figure 11, was insignificant. The DIA method could potentially be recommended when quick results are needed for quality control purposes of the shape of the crushed fine particles down to about $40 \mu\text{m}$ in size at the crushed aggregate quarries. We emphasize that this point could only be concluded since the DIA method was checked against the more accurate 3-D $\mu\text{CT SH}$ method. For more complete information, especially at smaller particle sizes, the 3-D $\mu\text{CT SH}$ method with an appropriate scanner resolution is recommended instead of the DIA method;
- While the mean shape of 2-D projections do empirically correlate reasonably well with 3-D measurements, at least in terms of the L/W ratio, the two measurements are not the same and the correlation is only empirical.

ACKNOWLEDGEMENTS

This work is based on work performed in COIN – Concrete Innovation Centre (www.coinweb.no) – which is a Centre for Research based Innovation, initiated by the Research Council of Norway (RCN) in 2006. The authors would like to gratefully acknowledge COIN for financial support and for facilitating the interaction between research and industry. As well, help of lab engineer Steinar Seehuus with preparation of the epoxy casted specimens for μCT scanning is greatly appreciated.

REFERENCES

- [1] B. Wigum, S. Danielsen, O. Hotvedt og B. Pedersen, «Production and utilisation of

- manufactured sand. COIN project report 12-2009,» SINTEF, Trondheim, 2009.
- [2] M. Westerholm, B. Lagerblad, J. Silfwerbrand and E. Forsberg, “Influence of fine aggregate characteristics on the rheological properties of mortars,” *Cement and Concrete Composites*, vol. 30, no. 4, p. 274–282, 2008.
- [3] M. Westerholm and B. Lagerblad, “Filler and filler quality of crushed rocks in concrete production,” in *International Conference on Building Materials "18. ibausil"*, Weimar, Germany, 12th-15th of September, 2012.
- [4] B. Lagerblad, H.-E. Gram og M. Westerholm, «Evaluation of the quality of fine materials and filler from crushed rocks in concrete production,» *Construction and Building Materials*, vol. 67, pp. 121-126, 2014.
- [5] Anonymous, «Banyan: Such quantities of sand. Asia’s mania for “reclaiming” land from the sea spawns mounting problems,» *The Economist*, vol. March, p. 35, 2015.
- [6] R. Cepuritis, “New type of crushed sand to replace natural sand in concrete production,” *Metso's customer magazine for the mining and construction industries - results: minerals&aggregates*, vol. 2, pp. 38-43, 2014.
- [7] R. Cepuritis, “Effects of Concrete Aggregate Crushing on Rheological Properties of Concrete and Matrix. Master thesis,” Norwegian Univeristy of Science and Technology, 2011.
- [8] R. Cepuritis, “Building on Sand,” *International Cement Review*, no. December, pp. 81-83, 2014.
- [9] R. Cepuritis, “From Stockpile to Sand,” *Quarry*, no. July, pp. 22-28, 2014.
- [10] R. Cepuritis, “Sand from the Rocks. New type of crushed sand to replace natural sand in concrete production,” *Bulk Solids Handling*, vol. 3, pp. 42-48, 2014.
- [11] N. Ahn, “An experimental study on the guidelines for using higher contents of aggregate micro fines in Portland cement concrete. PhD,” The University of Texas, 2000.
- [12] P. Quiroga, “The effect of the aggregate characteristics on the performance of Portland cement concrete,” The University of Texas, 2003.
- [13] D. Cortes, H.-K. Kim, A. Palomino and J. Santamarina, “Rheological and mechanical properties of mortars prepared with natural and manufactured sands,” *Cement and Concrete Research*, pp. 1142-1147, 2008.
- [14] R. Cepuritis, S. Jacobsen, B. Pedersen and E. Mørtzell, “Crushed sand in concrete –

- effect of particle shape in different fractions and filler properties on rheology,” *Cement and Concrete Composites*, vol. 71, pp. 26-41, 2016.
- [15] E. Hämäläinen, “Manufactured sand success with Velde Pukk in Norway,” *Metso's customer magazine for the mining and construction industries - results: minerals&aggregates*, vol. 2, pp. 6-7, 2010.
- [16] D. Morrow, «Why manufactured sand?,» *Metso's customer magazine for the mining and construction industries - results: minerals&aggregates*, vol. 1, pp. 26-27, 2011.
- [17] H. Pettingel, «An effective dry sand manufacturing process from Japan. Potential to replace natural sand entirely in concrete,» *Quarry Management Magazine*, vol. June, pp. 1-6, 2008.
- [18] T. Kaya, «The development of sand manufacture from crushed rock in Japan, using advanced VSI technology. Importance of fine aggregate shape and grading on properties of concrete,» i *Proceedings of 17th Annual Symposium of International Centre for Aggregates Research*, Austin, Texas, 2009.
- [19] Robo Silicon, «The Future of Sand is Here,» 2014. [Internett]. Available: http://www.robo.co.in/Download_RoboSand.pdf. [Funnet 09 12 2014].
- [20] Sandvik Rock Processing, «Merlin-VSI(TM) setting the standard in VSI crushing,» [Internett]. Available: [http://www.miningandconstruction.sandvik.com/sandvik/9082/Internet/S002630.nsf/Alldocs/Products*5CCrushers*and*screens*5CVSI*impact*crushers*2ARP106/\\$file/Merlin%20VSI%20ENG.pdf](http://www.miningandconstruction.sandvik.com/sandvik/9082/Internet/S002630.nsf/Alldocs/Products*5CCrushers*and*screens*5CVSI*impact*crushers*2ARP106/$file/Merlin%20VSI%20ENG.pdf). [Funnet 09 12 2014].
- [21] M. Bengtsson, «Quality-Driven Production of Aggregates in Crushing Plants,» Chalmers University of Technology. PhD, 2009.
- [22] M. Bengtsson og C. Evertsson, «Measuring characteristics of aggregate material from vertical shaft impact crushers,» *Minerals Engineering*, vol. 19, pp. 1479-1486, 2006.
- [23] U. Åkesson og B. Tjell, «Geological parameters controlling the improvement of manufactured sand using vertical shaft impact crushers instead of cone crushers,» i *XXV International Mineral Processing Congress (IMPC) 2010*, Brisbane, QLD, Australia, 6th to 10th of September 2010, 2010.
- [24] M. Bengtsson, P. Svedensten og C. Evertsson, «Improving yield and shape in a crushing plant,» *Minerals Engineering*, vol. 22, pp. 618-624, 2009.
- [25] M. Bengtsson og E. C.M., «Modelling of output and power consumption in vertical

- shaft impact crushers,» *International Journal of Mineral Processing*, vol. 88, pp. 18-23, 2008.
- [26] M. Ramos, M. Smith og T. Kojovic, «Aggregate shape: prediction and control during crushing,» *Quarry Management*, nr. November, pp. 23-30, 1994.
- [27] R. Cepuritis, S. Jacobsen and T. Onnela, “Sand production with VSI crushing and air classification: optimizing fines grading for concrete production with micro-proportioning,» *Minerals Engineering*, vol. 78, pp. 1-14, 2015.
- [28] American Society for Testing and Materials, «ASTM D4791-10 Standard Test Method for Flat Particles, Elongated Particles, or Flat and Elongated particles in Coarse Aggregate,» ASTM, Pennsylvania, 2010.
- [29] European Committee for Standardization, “EN 933-3:2012 Tests for geometrical properties of aggregates - Part 3: Determination of particle shape - Flakiness index,» CEN, Brussels, 2012.
- [30] European Committee for Standardization, “EN 933-4:2008 Tests for geometrical properties of aggregates. Part 4: Determination of particle shape. Shape index,» CEN, Brussels, 2008.
- [31] B. Lagerblad, “Crushed rock as aggregate for concrete. Final report. MinBaS project No. 2.2 Future concrete- Subproject 2.23 Utilization of alternative types of aggregates in concrete. MinBaS Area 2. Report 2:19.,” MinBaS, Stockholm (In Swedish), 2005.
- [32] M. Westerholm, «Rheology of the Mortar Phase of Concrete with Crushed Aggregate. Licentiate thesis,» Luleå University of Technology, 2006.
- [33] H. Merkus, *Particle Size Measurements: Fundamentals, Practice, Quality.*, Dordrecht: Springer Netherlands, 2009.
- [34] P. Gottlieb, G. Wilkie, D. Sutherland, E. Ho-Tun, S. P. K. Suthers, B. Jenkins, S. Spencer, A. Butcher og J. Rayner, «Using quantitative electron microscopy for process mineralogy applications,» *JOM*, vol. 52, nr. 4, pp. 24-25, 2000.
- [35] A. Laskin og J. Cowin, «Automated Single-Particle SEM/EDX Analysis of Submicrometer Particles down to 0.1 μm ,» *Anal. Chem.*, vol. 73, nr. 5, pp. 1023-1029, 2001.
- [36] D. Pirre, A. Butcher, M. Power, P. Gottlieb og G. Miller, «Rapid quantitative mineral and phase analysis using automated scanning electron microscopy (QemSCAN); potential applications in forensic geoscience,» *Geological Society London, Special*

- Publication*, vol. 232, pp. 123-136, 2004.
- [37] E. Garboczi, "Three-dimensional mathematical analysis of particle shape using x-ray tomography and spherical harmonics: application to aggregates used in concrete," *Cement and Concrete Research*, vol. 32, pp. 1621-1638, 2002.
- [38] S. Erdoğan, P. Quiroga, D. Fowler, H. Saleh, R. Livingston, E. Garboczi, P. Ketcham, J. Hagedorn and S. Satterfield, "Three-dimensional shape analysis of coarse aggregates: new techniques for and preliminary results on several different coarse aggregates and reference rocks," *Cement and Concrete Research*, vol. 36, pp. 1619-1627, 2006.
- [39] M. A. Taylor, E. J. Garboczi, S. T. Erdoğan and D. W. Fowler, "Some properties of irregular 3-D particles," *Powder Technology*, no. 162, pp. 1-15, 2006.
- [40] E. Masad, S. Saadeh, T. Al-Rousan, E. Garboczi and D. Little, "Computations of particle surface characteristics using optical and x-ray CT images," *Journal of Computational Materials Science*, vol. 34, pp. 406-424, 2005.
- [41] E. Garboczi and J. Bullard, "Shape analysis of a reference cement," *Cement and Concrete Research*, vol. 34, pp. 1933-1937, 2004.
- [42] G. Cheok, W. Stone and E. Garboczi, "Using LADAR to characterize the 3D shape of aggregates: preliminary results," *Cement and Concrete Research*, vol. 36, pp. 1072-1075, 2006.
- [43] S. T. Erdoğan, E. J. Garboczi and D. W. Fowler, "Shape and size of microfine aggregates: X-ray microcomputed tomography vs. laser diffraction," *Powder Technology*, no. 177, pp. 53-63, 2007.
- [44] L. Holzer, R. Flatt, S. Erdoğan, J. Bullard and E. Garboczi, "Shape comparison between 0.4 μm to 2.0 μm and 20 μm to 60 μm cement particles," *Journal of American Concrete Society*, vol. 93, pp. 1626-1633, 2010.
- [45] S. Erdoğan, X. Nie, P. Stutzman and E. Garboczi, "Micrometer-scale 3D shape characterization of eight cements: particle shape and cement chemistry, and the effect of particle shape on laser diffraction particle size measurement," *Cement and Concrete Research*, vol. 40, pp. 731-739, 2010.
- [46] E. Garboczi, "Three dimensional shape analysis of JSC-1A simulated lunar regolith particles," *Powder Technology*, vol. 207, pp. 96-103, 2011.
- [47] E. Garboczi and A. Haleh, "National Cooperative Highway Research Program 20-07

- (243): Development of Glass Beads Utilised in Traffic Markings,” Transportation Research Board, Washington, 2010.
- [48] R. Cepuritis, B. Wigum, E. Garboczi, E. Mørtzell and S. Jacobsen, “Filler from crushed aggregate for concrete: Pore structure, specific surface, particle shape and size distribution,” *Cement and Concrete Composites*, vol. 54, pp. 2-16, 2014.
- [49] R. Cepuritis, E. Garboczi, C. Ferraris, F. Jacobsen and B. Sørensen, “Measurement of particle size distribution and specific surface area for crushed concrete aggregate fines,” *Manuscript submitted for publication to Cement and Concrete Composites*.
- [50] R. Cepuritis, E. Garboczi og S. Jacobsen, «Three dimensional shape analysis of concrete aggregate fines produced by VSI crushing,» *Manuscript submitted for publication to Powder Technology*, 2016.
- [51] AnaTec, «FPA. Fine Particle Analyser,» [Internett]. Available: http://www.ana-tec.com/website/_images/produkte/fpa/FPA_English.pdf.
- [52] E. Garboczi, X. Liu and M. Taylor, “The 3-D shape of blasted and crushed rocks: From 20 μm to 38 mm,” *Powder Technology*, vol. 229, pp. 84-89, 2012.
- [53] J. Bullard and E. Garboczi, “Defining shape measures for 3-D star-shaped particles: sphericity, roundness, and dimensions,” *Powder Technology*, no. 249, pp. 241-252, 2013.
- [54] E. Garboczi and J. Bullard, “Contact function, uniform-thickness shell volume, and convexity measure for 3-D star-shaped particles,” *Powder Technology*, no. 237, pp. 191-201, 2013.
- [55] E. J. Garboczi, «Three-dimensional mathematical analysis of particle shape using X-ray tomography and spherical harmonics: application to aggregates used in concrete,» *Cement and Concrete Research*, vol. 32, nr. 10, pp. 1621-1638, 2002.
- [56] American Society for Testing and Materials, “Standard Test Method for Flat Particles, Elongated Particles, or Flat and Elongated particles in Coarse Aggregate,” ASTM, Pennsylvania, ASTM D4791-10.
- [57] W. Krumbein, “Measurement and geological significance of shape and roundness of sedimentary particles,” *Journal of Sedimentary Petrology*, vol. 11, pp. 64-72, 1941.
- [58] J. Fonseca, «The evolution of morphology and fabric of a sand during shearing,» Imperial College, London, 2011.
- [59] J. Fonseca, C. O'Sullivan, M. Coop og P. Lee, «Non-invasive characterization of

- particle morphology of natural sands,» *Soils and Foundations*, vol. 52, nr. 4, pp. 712-22, 2012.
- [60] B. Aschenbrenner, “A new method of expressing particle sphericity,” *Journal of sedimentary petrology*, vol. 26, pp. 15-31, 1956.
- [61] T. Powers, *The Properties of Fresh Concrete*, New York: John Wiley & Sons, 1968.
- [62] E. Parteli, «Attractive particle interaction forces and packing density of fine glass powders,» *Scientific Reports*, vol. 4, pp. 1-7, 2014.
- [63] A. Yu, J. Bridgwater og A. Burbidge, «On the modelling of the packing of fine particles,» *Powder Technology*, vol. 92, pp. 185-194, 1997.
- [64] M. Götzinger og W. Peukert, «Dispersive forces of particle-surface interactions: direct AFM measurements and modelling,» *Powder Technology*, vol. 130, pp. 102-109, 2003.
- [65] M. Götzinger og W. Peukert, «Particle Adhesion Force Distribution on Rough Surface,» *Langmuir*, vol. 20, pp. 5298-5303, 2004.
- [66] A. Castellanos, «The relationship between attractive interparticle forces and bulk behaviour in dry and uncharged fine powders,» *Advances in Physics*, vol. 54, pp. 263-376, 2005.
- [67] Q. Li, V. Rudolph og W. Peukert, «London-van der Waals adhesiveness of rough-surfaced particles,» *Powder Technology*, vol. 161, pp. 248-255, 2006.
- [68] E. Underwood, *Quantitative Stereology*, Boston: Addison-wesley, 1970.
- [69] D. Gendzwill og M. Stauffer, «Analysis of Triaxial Ellipsoids: Their Shapes, Plane Sections, and Plane Projections,» *Mathematical Geology*, vol. 13, nr. 2, pp. 135-152, 1981.
- [70] European Committee for Standardization, «EN 12620:2008 Aggregates for concrete,» CEN, Brussels, 2008.
- [71] American Society for Testing and Materials, «ASTM C33 / C33M - 13 Standard Specification for Concrete Aggregates,» ASTM, 2013.
- [72] E. Mørtzell, «Modelling the effect of concrete part materials on concrete consistency. PhD,» Norwegian University of Science and Technology (In Norwegian), 1996.
- [73] P. Billberg, «Some rheology aspects of fine mortar part of concrete,» KTH Royal Institute of Technology. Lic. thesis, 1999.



Dr. **Rolands Cepuritis** is a Post-Doctoral Fellow at the Norwegian University of Science and Technology and a project manager at the Norwegian cement producer Norcem. He has ten years of practical experience in fields of aggregate, cement and concrete production, concrete structure contracting and research. He is an author of more than 30 publications related to his fields of experience. He was awarded the Kristaps Morbergs Engineering Scholarship from the University of Latvia in 2008 and a European Social Fund Master Student Scholarship in 2010. Dr. Cepuritis is a member of RILEM.



Dr. **Edward J. Garboczi** is a NIST (National Institute of Science and Technology) Fellow in the Applied Chemicals and Materials Division and has published more than 140 papers. He is a member of the American Physical Society, the American Ceramic Society, and the American Concrete Institute (ACI). He received the Robert L'Hermite Medal from RILEM in 1992, a Silver Medal from the Department of Commerce in 2009, the 2012 Della Roy Lecture award from the American Ceramic Society, and the 2014 Robert Philleo award from ACI. He is a Fellow of both the American Ceramic Society and ACI.



Dr. **Stefan Jacobsen** is a professor at the Norwegian University of Science and Technology, Department of Structural Engineering, where he teaches an M.Sc. level course in Concrete Technology and a PhD level course - Concrete: Structure-Property Relationship. Previously, he has held a professor position at Narvik College, researcher positions at different research institutes in Norway, and worked in the contracting business. He is a member of the ISO TC 71/SC8 Environmental management for concrete and concrete structures, RILEM TC-FPC Formwork pressure, the Norwegian Concrete Association and the Concrete Innovation Centre. Dr. Jacobsen is author of more than 90 publications.



Dr. **Kenneth A. Snyder** is the Deputy Division Chief of the Materials and Structural Systems Division (MSSD) of the

Engineering Laboratory (EL) at the National Institute of Standards and Technology (NIST). He is author of more than 60 scientific publications. In 2009, Dr. Snyder and Dale Bentz were awarded a U.S. Department of Commerce Bronze Medal award for their research on developing a new class of concrete admixtures to slow diffusion in cement-based materials based on nanoscale viscosity modifiers. Dr. Snyder is a member of the following professional societies: American Physical Society (APS), ASTM International, and RILEM.

ACCEPTED MANUSCRIPT

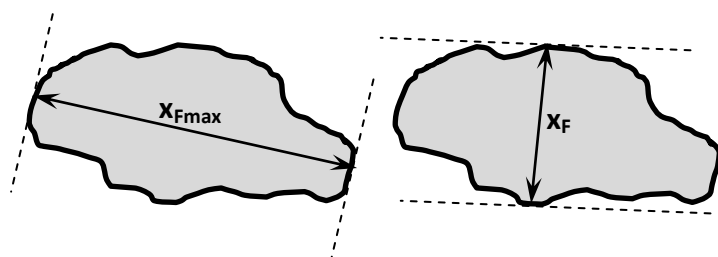


Fig. 1

ACCEPTED MANUSCRIPT

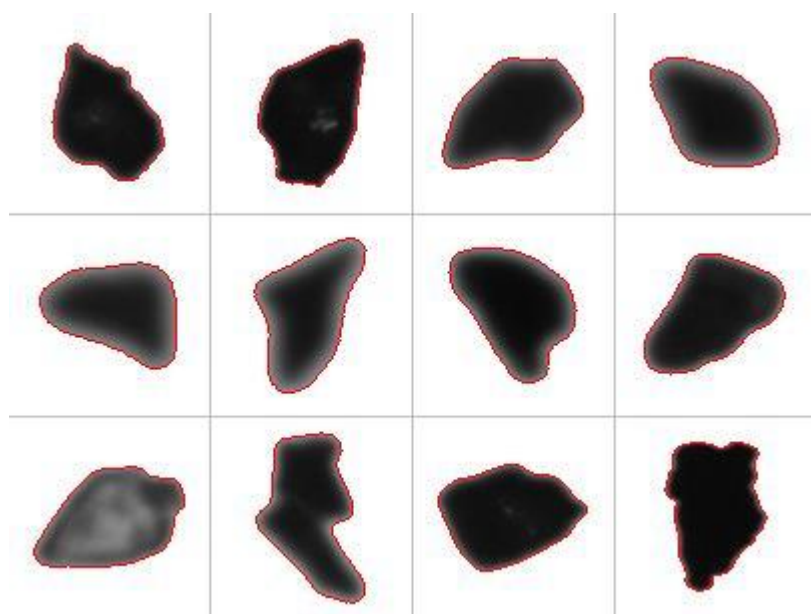


Fig. 2

ACCEPTED MANUSCRIPT

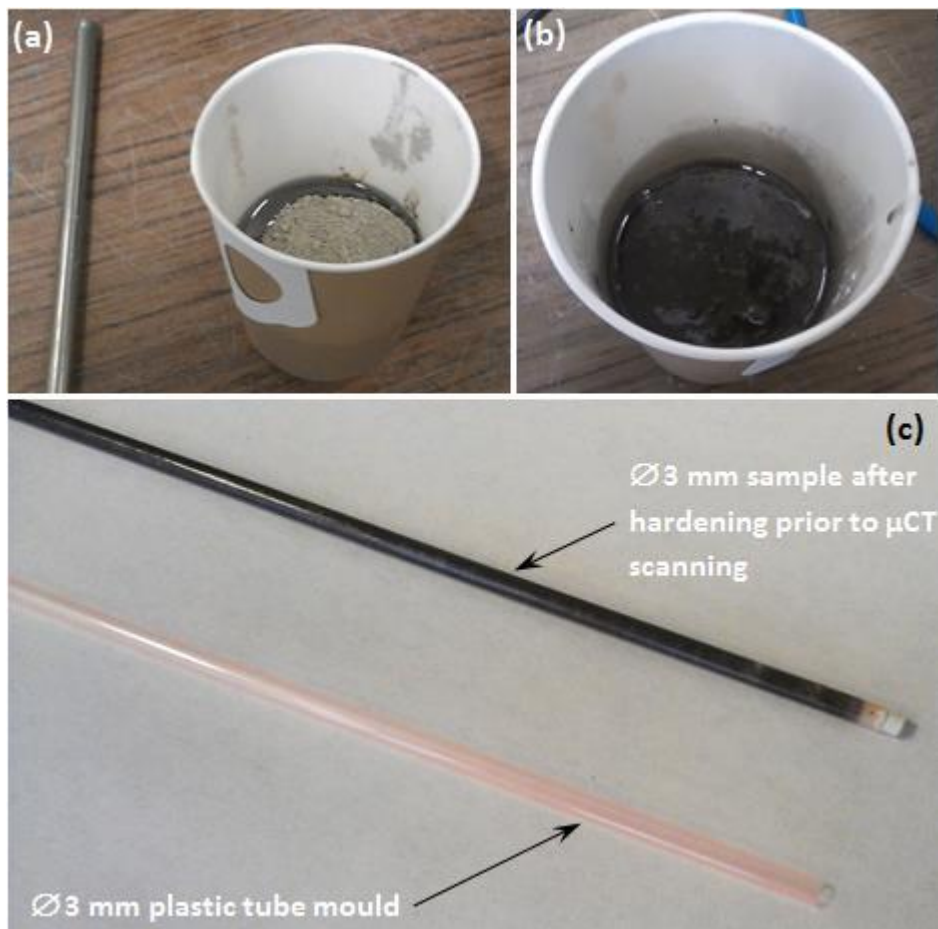


Fig. 3

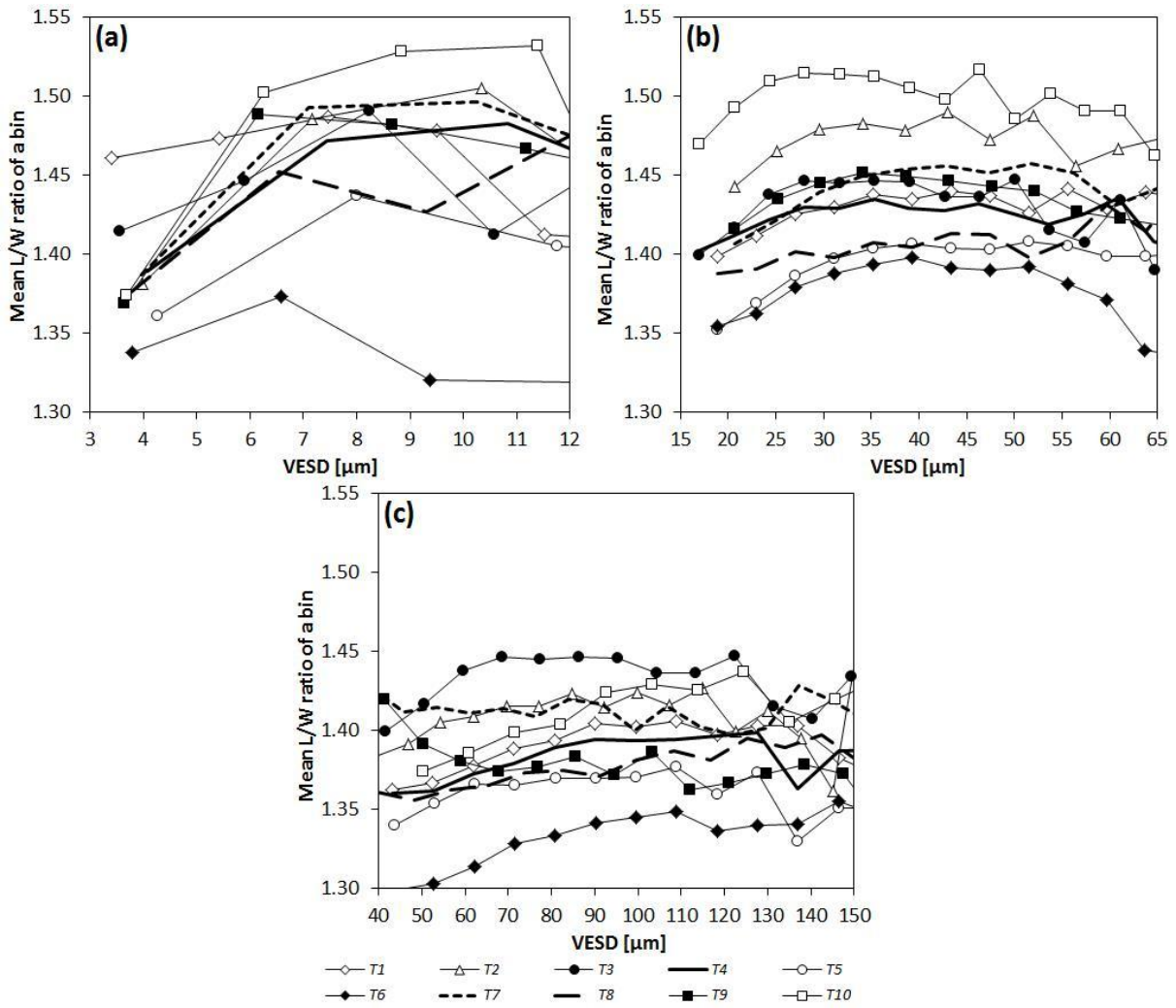


Fig. 4

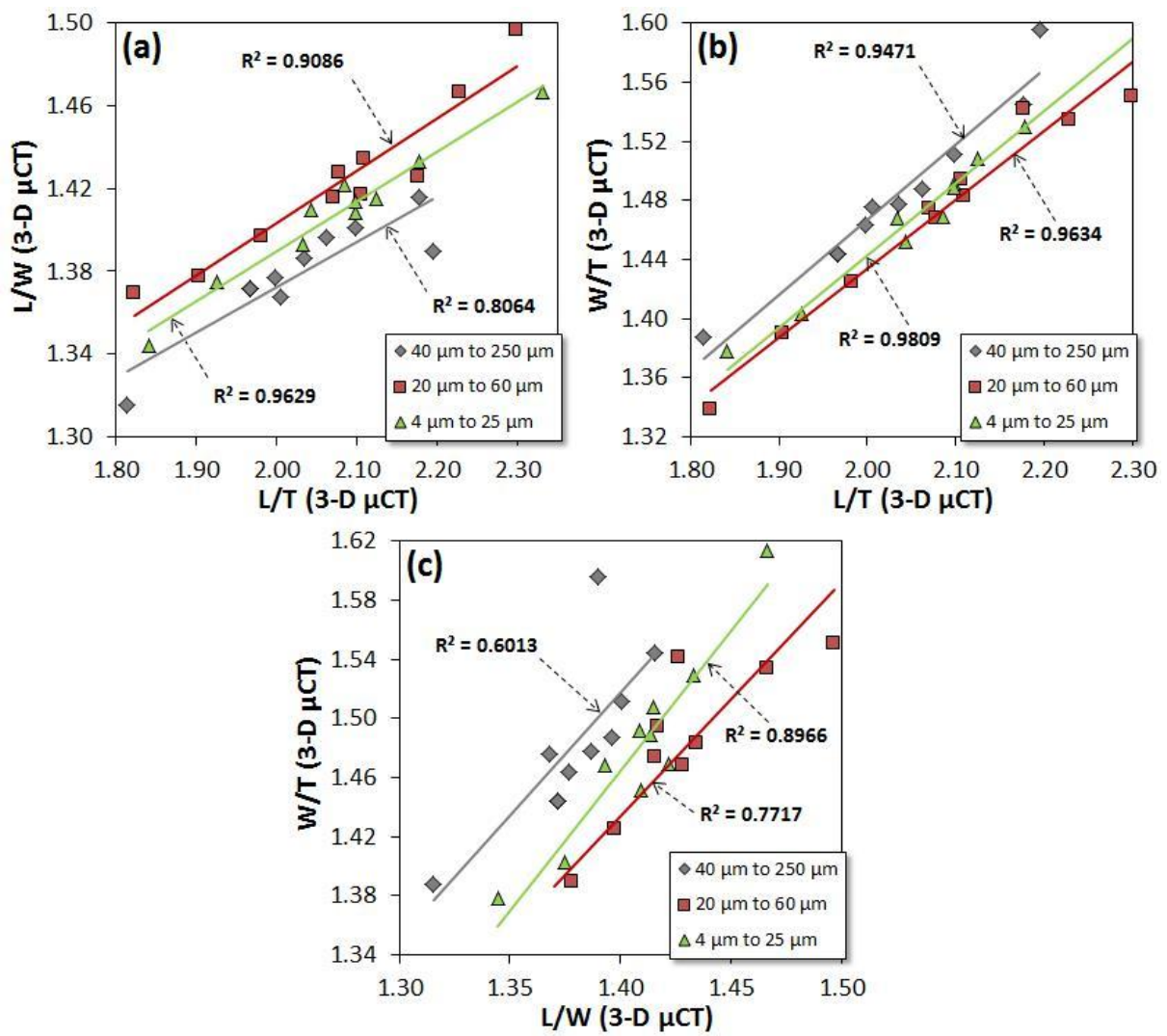


Fig. 5

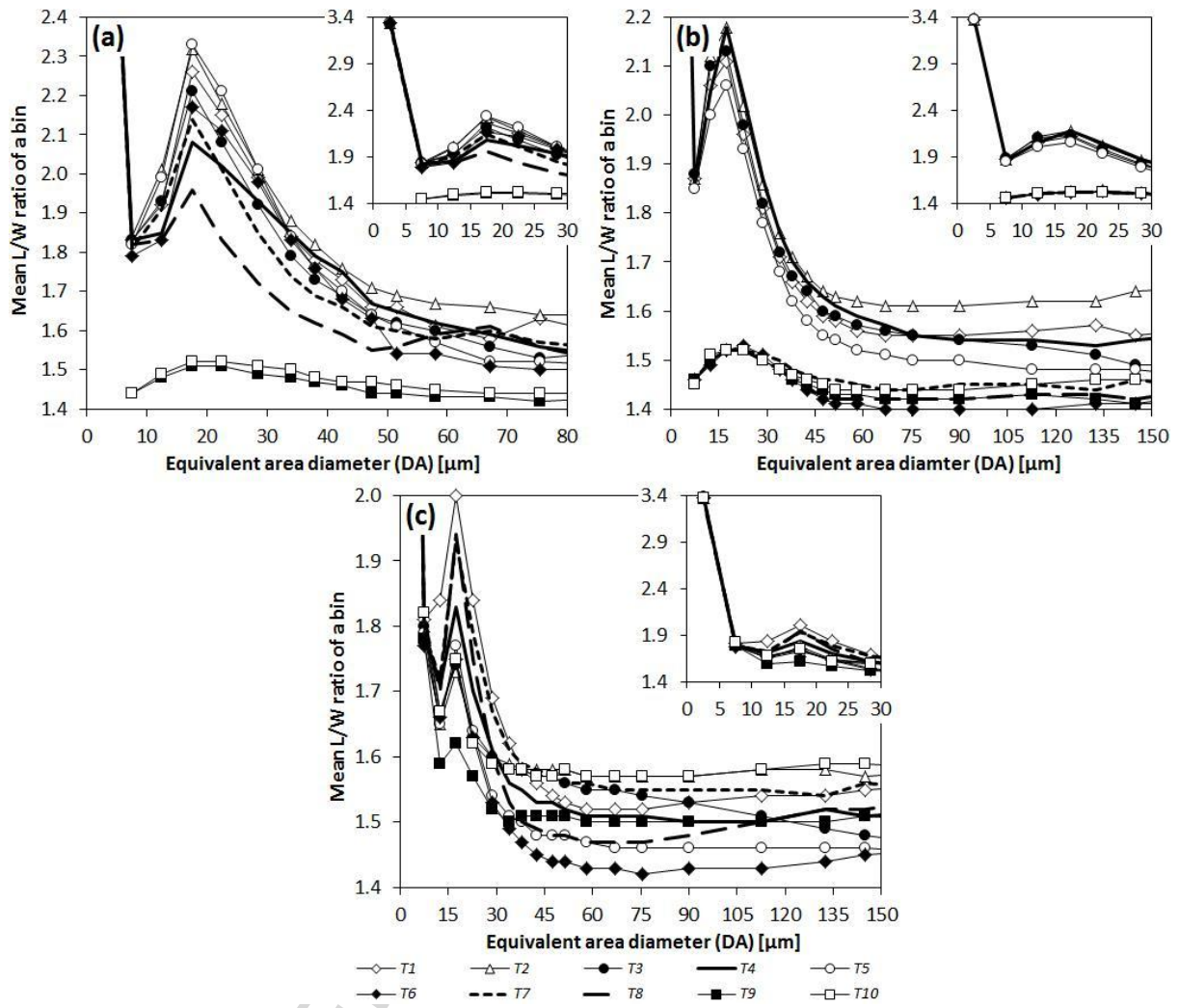


Fig. 6

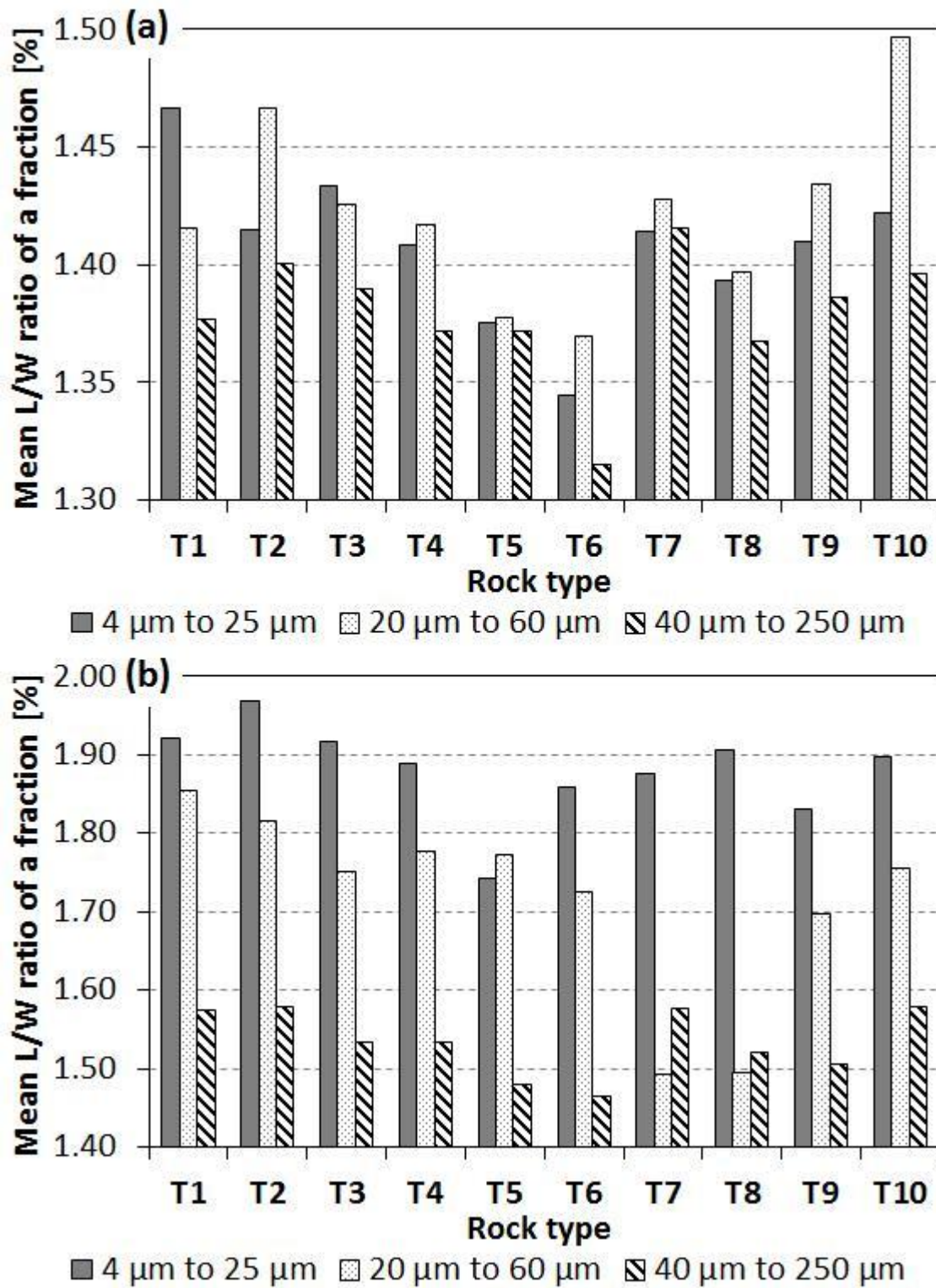


Fig. 7

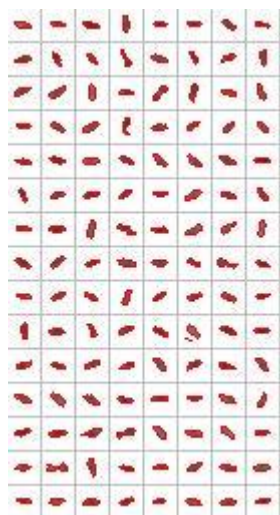


Fig. 8

ACCEPTED MANUSCRIPT

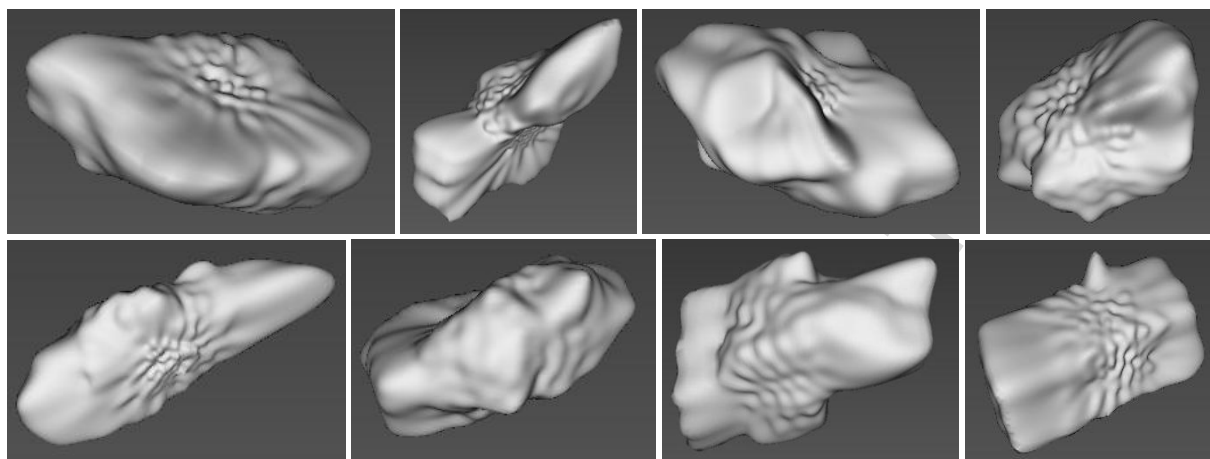


Fig. 9

ACCEPTED MANUSCRIPT

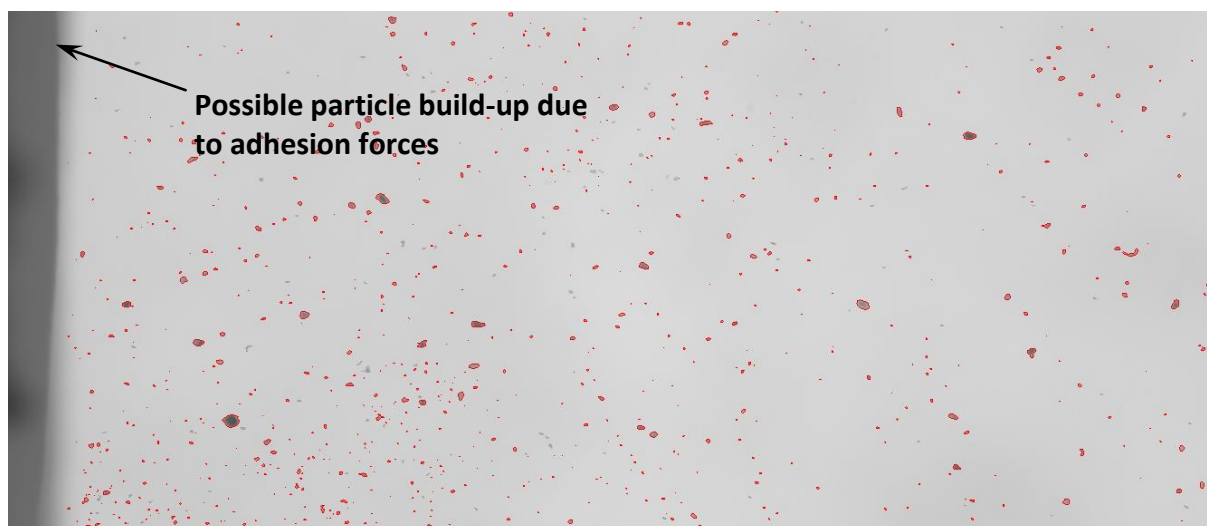


Fig. 10

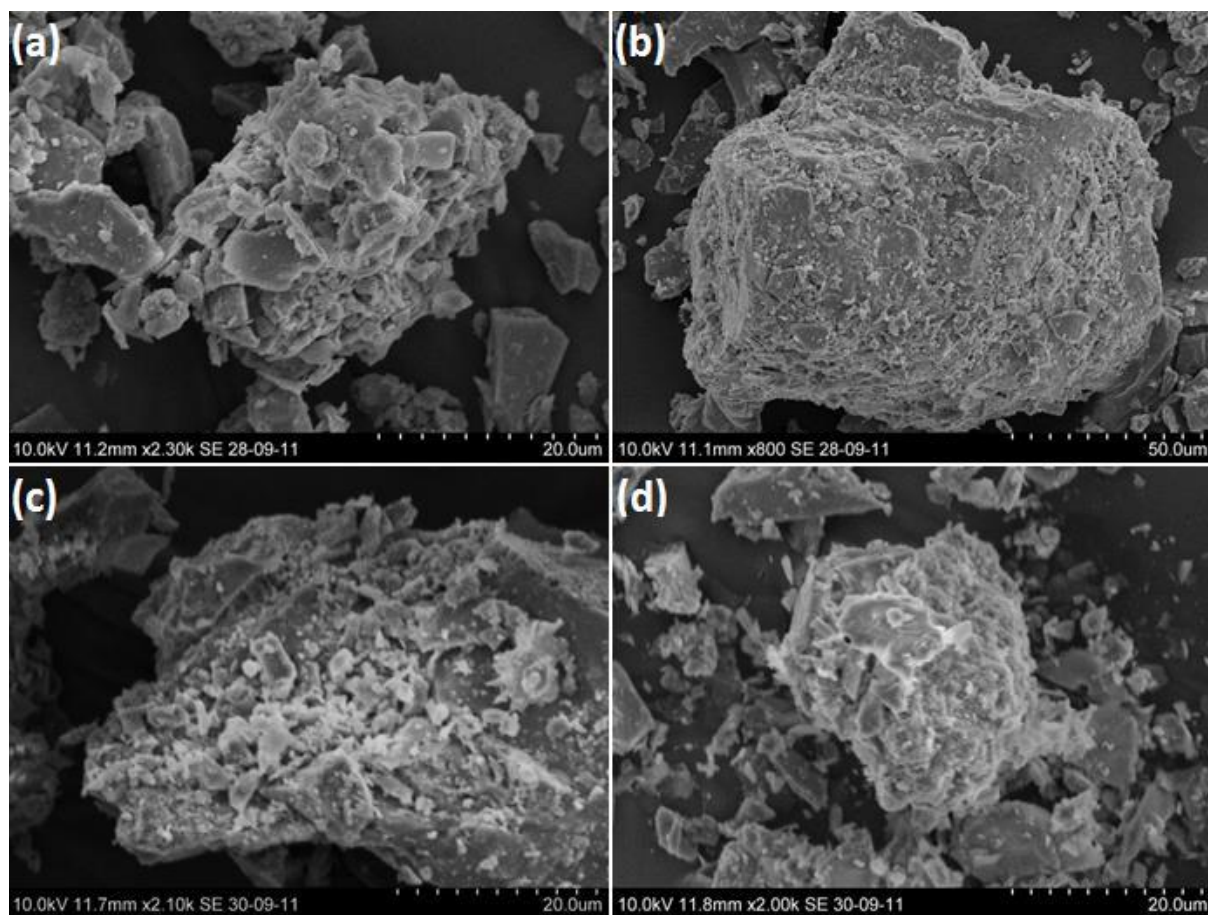


Fig. 11

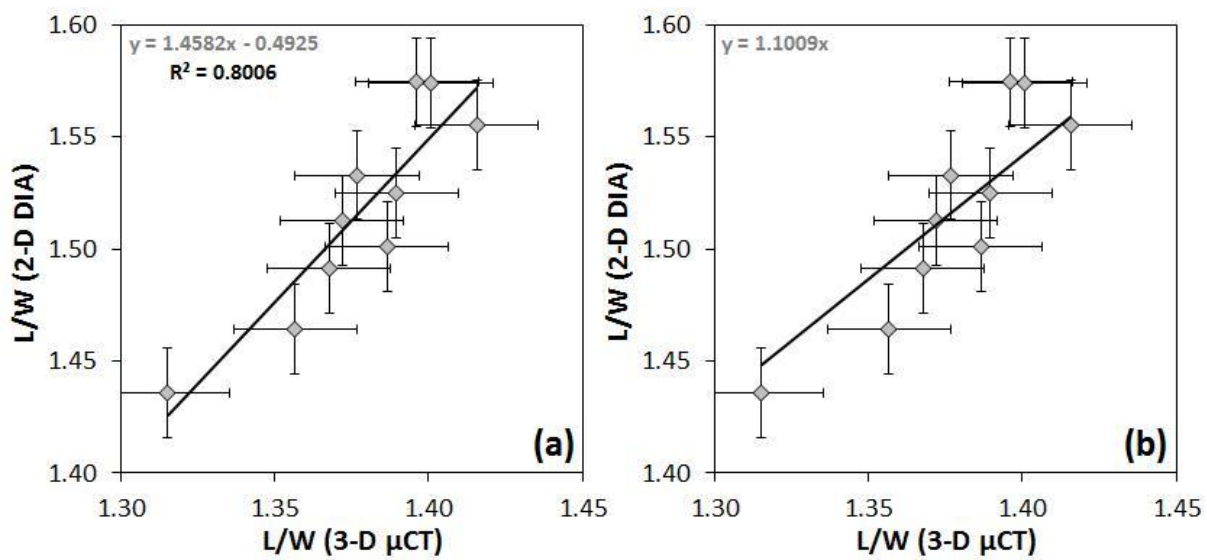


Fig. 12

ACCEPTED MANUSCRIPT

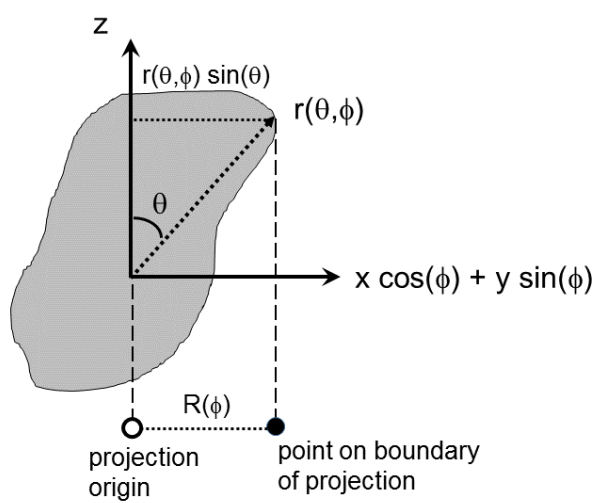


Fig. 13

ACCEPTED MANUSCRIPT

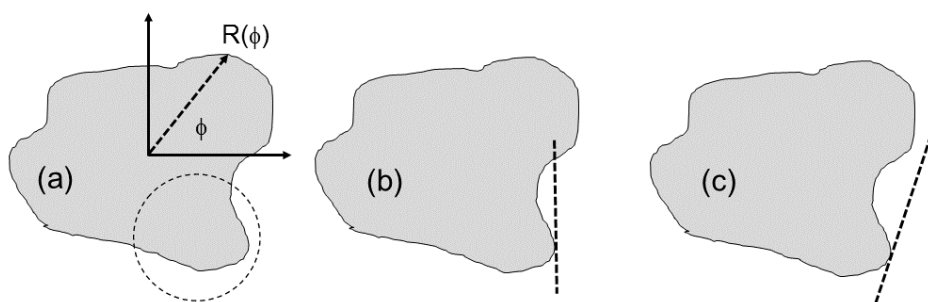


Fig. 14

ACCEPTED MANUSCRIPT

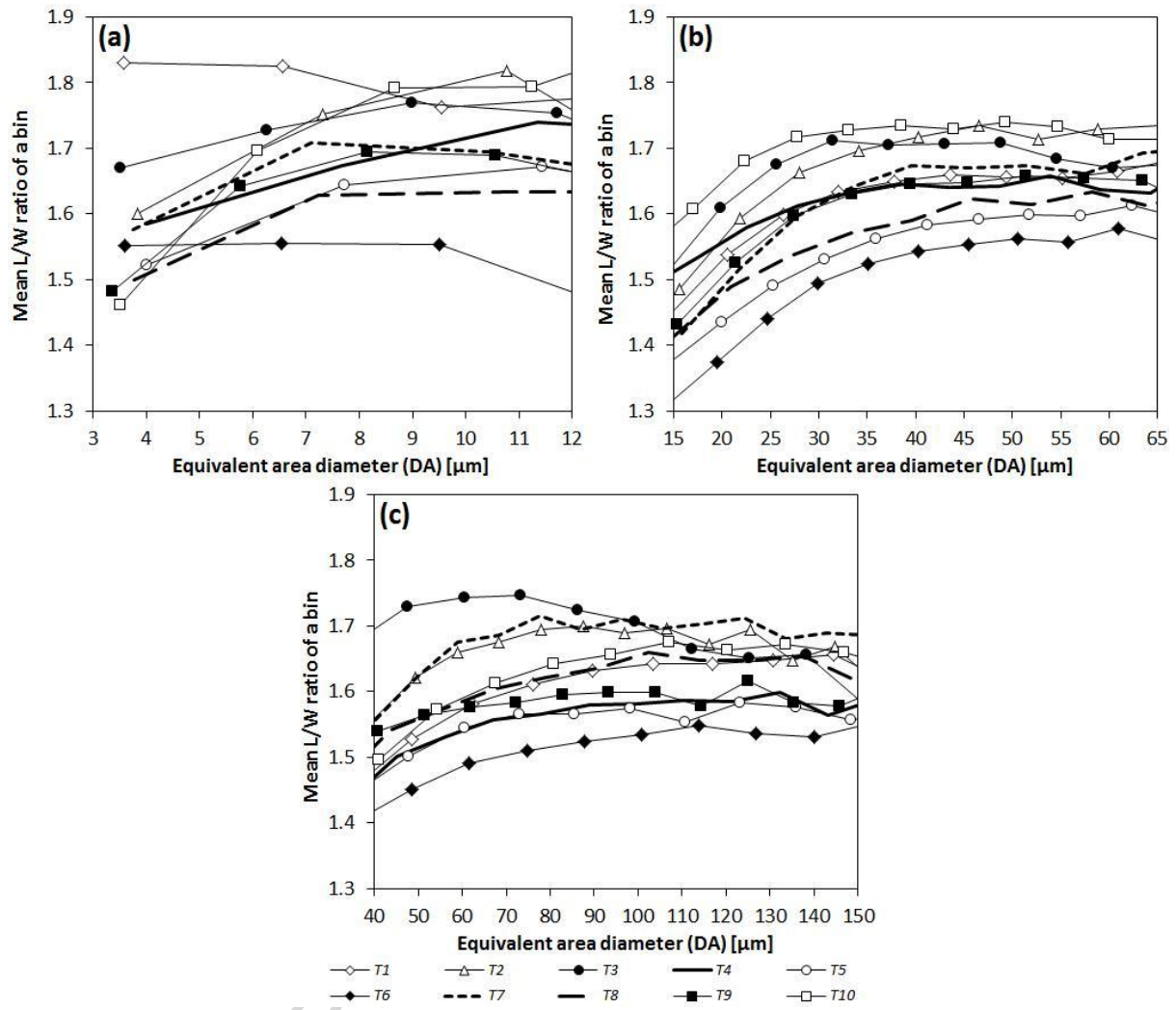


Fig. 15

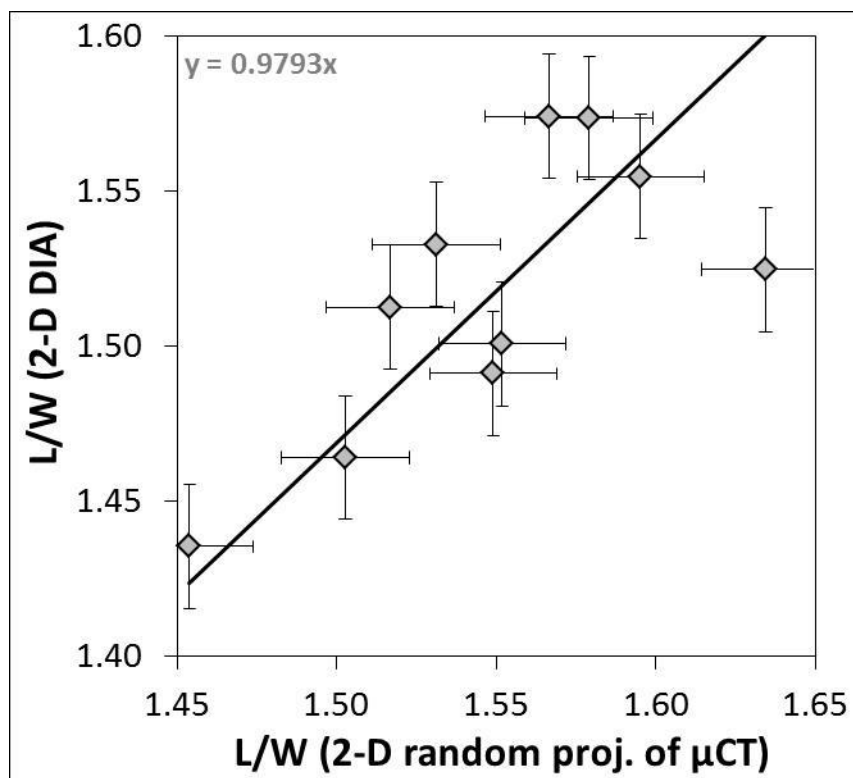


Fig. 16

Table 1: Crushed rock fines used for the study.

Rock type designation	Rock name	Rock type	Mono- or multiminerallc	Crushed rock fines fraction				
				Crushability ^a	Los Angeles value ^b	Fine	Medium	Coarse
						[%]	[%]	4 μm to 25 μm
T1	Mylonitic quartz diorite	Metamorphic	Multiminerallc	23	12	T1-1	T1-2	T1-3
T2	Gneiss/granite ^d	Metamorphic/ igneous (intrusive)	Multiminerallc	41	20	T2-1	T2-2	T2-3
T3	Quartzite	Metamorphic	Monominerallc	49	25	T3-1	T3-2	T3-3
T4	Anorthosite	Igneous (intrusive)	Multiminerallc	28	14	T4-1	T4-2	T4-3
T5	Limestone	Sedimentary	Monominerallc ^c	45	22	T5-1	T5-2	T5-3
T6	Limestone	Sedimentary	Multiminerallc ^c	36	18	T6-1	T6-2	T6-3
T7	Dolomite	Sedimentary	Multiminerallc	98	92	T7-1	T7-2	T7-3
T8	Basalt	Igneous (extrusive)	Multiminerallc	18	11	T8-1	T8-2	T8-3
T9	Aplite	Igneous (intrusive)	Multiminerallc	40	20	T9-1	T9-2	T9-3
T10	Granitic gneiss	Igneous (intrusive)/ metamorphic	Multiminerallc	54	29	T10-1	T10-2	T10-3

^a Determined according to the French standard NF P18-579 (1990) [51], [27].

^b The Los Angeles values according to EN 1097-2 [52] have been approximated from the crushability testing results using the correlation relationship available in [53].

^c According to the XRD analysis results (Table 2) T5 and T6 have 95 % to 97 % carbonate minerals. However, while T5 has 97 % limestone (CaCO₃), T6 has 74.5 % limestone (CaCO₃) and 20.5 % dolomite minerals (CaMg(CO₃)₂) and thus cannot be considered monomineralic.

^d The material was obtained from a natural gravel deposit and consisted of a mix of mainly gneiss and granite rock types.

Table 2: Mineralogical composition of the various rock types used, determined with quantitative XRD.

Rock type	Mylonitic quartz diorite	Gneiss/ granite	Quartzite	Anorthosite	Limestone	Limestone	Dolomite	Basalt	Aplite	Granite/ gneiss
Rock type designation	T1	T2	T3	T4	T5	T6	T7	T8	T9	T10
Tested size fraction	4 μm to 25 μm									
Mineral or group of minerals	Mass %									
Quartz	27.9	20.9	90.0	6.5	2.3	2.5	1.1	8.9	36.2	17.8
Carbonate minerals	4.4	-	3.6	10.6	97.7	95.0	95.0	8.3	-	5.0
Epidote minerals	8.4	-	-	24.4	-	-	-	7.6	-	-
Feldspar minerals	37.7	63.9	3.9	33.1	-	0.4	0.6	26.5	58.2	58.8
Sheet silicates (micas ^a)	1.3	3.7	1.5	-	-	1.1	-	5.2	2.7	5.5
Sheet silicates (other)	6.7	4.4	-	20.4	-	0.4	0.7	0.0	0.0	3.7
Chlorite	11.3	1.4	1.0	2.6	-	0.6	1.6	20.2	1.7	0.5
Inosilicate minerals	1.0	3.9	-	2.3	-	-	1.1	11.0	1.2	8.7
Iron oxide minerals	-	-	-	-	-	-	-	3.5	-	-
Other minerals	1.3	1.9	-	0.2	-	-	-	8.8	-	-

^a Biotite and muscovite.

Table 3: μ CT and SH analysis – pixel size, smallest analysed particle size, image size and number of analysed particles.

Fraction	4 μm to 25 μm	20 μm to 60 μm	40 μm to 250 μm
Average pixel size used for the μCT scanning [μm]	0.32	1.71	3.87
Smallest analysed particle size (VESD of a 512 voxel particle) [μm]	3.18	16.97	38.41
Image size [pixels]	ca. 900 x 968	2000 x 2000	2000 x 2000
Mean number of particles analysed	43 930	1 562 151	953 821

Table 4: Comparison of some particle characteristics of the T5-3 fines as determined from the 3-D shape analysis (columns 2-5) and from the 2-D projections of the 3-D μ CT SH particle models (columns 6-8). The 2-D projections in column 8 come from column 4 VRML images.

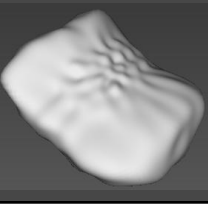
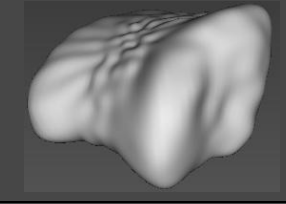
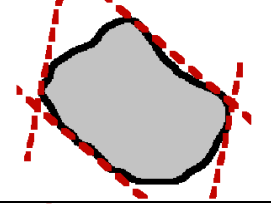
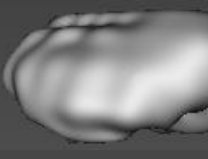
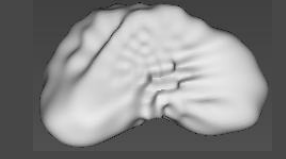

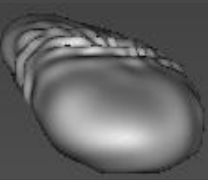
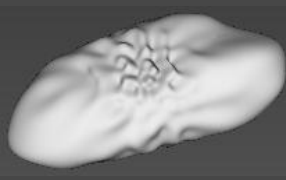
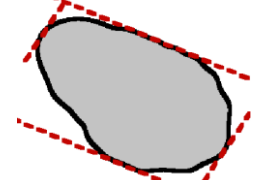
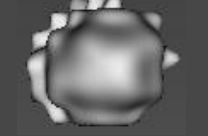


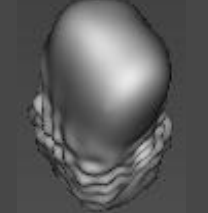
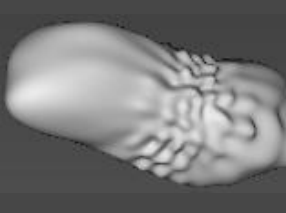
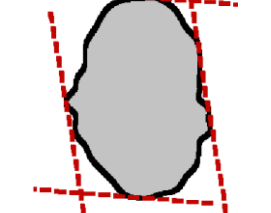
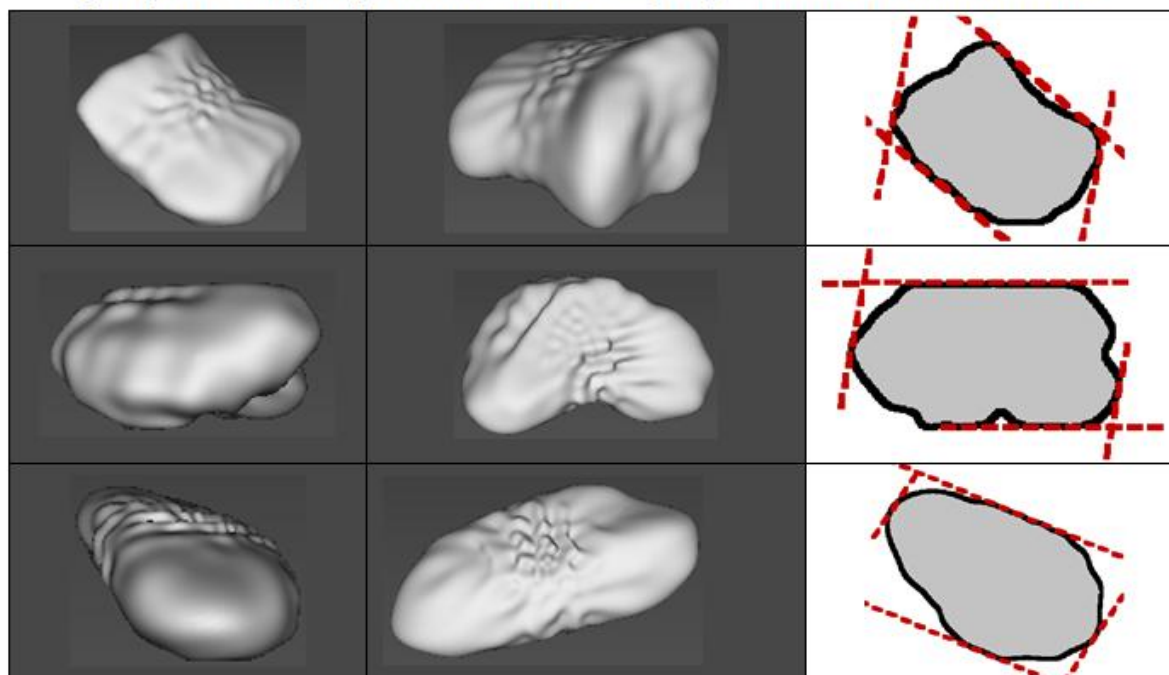
N o.	3-D μ CT SH results				2-D projections of 3-D SH models		
	VES D [μ m]	L/ W	Images of the actual particles based on the SH method of approximating the shape created with VRML		DA [μ m]	L/ W	Outline of the 2-D projections of the 3-D particles in the direction of z-axis and the measured Feret caliper distances
			As scanned, positive z-axis facing the viewer	Another characteristic view			
1	2	3	4	5	6	7	8
1.	103.6	1.00			116.3	1.46	
2.	61.3	1.50			52.1	1.89	
3.	79.1	2.00			67.9	1.70	
4.	40.1	2.50			30.2	1.13	
5.	82.2	3.03			68.74	1.42	

Table 5: Comparison of measured and calculated shadow (L/W) ratios for particles of 40 μm to 250 μm fractions using dynamic image analysis (DIA), μCT particles suspended in epoxy with and without orientation averaging, and ellipsoids having major axes equal to the major axes calculated from the μCT particles. The last column indicates the number of μCT particles used in the calculation.

Rock Type	2-D	2-D projections of 3-D data			
	DIA (L/W)	μCT (L/W), as scanned	μCT (L/W), random angle average	Ellipsoid (L/W)	Number of particles analysed
T1	1.53	1.55	1.53	1.52	190736
T2	1.57	1.61	1.58	1.56	130904
T3	1.52	1.71	1.63	1.60	38930
T4	1.51	1.53	1.52	1.50	117824
T5	1.46	1.52	1.50	1.49	91545
T6	1.44	1.47	1.45	1.43	126120
T7	1.55	1.62	1.60	1.59	100208
T8	1.49	1.59	1.55	1.52	50441
T9	1.50	1.57	1.55	1.53	57249
T10	1.57	1.60	1.57	1.55	49864

3-D μ CT & Spherical Harmonics crushed aggregate fine particle
(60 μm - 100 μm) models and 2-D projections of the models



Graphical abstract

ACCEPTED

Highlights:

- The 2-D DIA method is unable to measure shape of particles smaller than 40 μm .
- Main limitation of the 2-D DIA method is the pixel size and particle flocculation.
- The 2-D DIA method shows satisfying results for particles larger than 40 μm .

The 2-D DIA method is applicable for simple quality control at hard rock quarries.

ACCEPTED MANUSCRIPT